ARTICLES
https://doi.org/10.1038/s41590-022-01160-y

nature immunology

IL-1 and IL-1ra are key regulators of the inflammatory response to RNA vaccines

Siri Tahtinen[1], Ann-Jay Tong[1], Patricia Himmels[1], Jaehak Oh[1], Andres Paler-Martinez[1], Leesun Kim[1], Sara Wichner[1], Yoko Oei[1], Mark J. McCarron[1], Emily C. Freund[1], Zhainib Adel Amir[1], Cecile C. de la Cruz[1], Benjamin Haley[1], Craig Blanchette[1], Jill M. Schartner[1], Weilan Ye[1], Mahesh Yadav[1], Ugur Sahin[2], Lélia Delamarre[1] and Ira Mellman[1]✉

The use of lipid-formulated RNA vaccines for cancer or COVID-19 is associated with dose-limiting systemic inflammatory responses in humans that were not predicted from preclinical studies. Here, we show that the 'interleukin 1 (IL-1)–interleukin 1 receptor antagonist (IL-1ra)' axis regulates vaccine-mediated systemic inflammation in a host-specific manner. In human immune cells, RNA vaccines induce production of IL-1 cytokines, predominantly IL-1β, which is dependent on both the RNA and lipid formulation. IL-1 in turn triggers the induction of the broad spectrum of pro-inflammatory cytokines (including IL-6). Unlike humans, murine leukocytes respond to RNA vaccines by upregulating anti-inflammatory IL-1ra relative to IL-1 (predominantly IL-1α), protecting mice from cytokine-mediated toxicities at >1,000-fold higher vaccine doses. Thus, the IL-1 pathway plays a key role in triggering RNA vaccine-associated innate signaling, an effect that was unexpectedly amplified by certain lipids used in vaccine formulations incorporating N1-methyl-pseudouridine-modified RNA to reduce activation of Toll-like receptor signaling.

For adjuvanted vaccines, induction of an innate immune response is essential to generate a protective, long-lasting adaptive immune response. Capable of eliciting exceptionally strong T cell responses[1–3], RNA has emerged as an attractive vaccine platform not only for cancer therapy, but also for prophylaxis against infectious diseases such as COVID-19 (refs. [2–6]). RNA-based vaccines activate a range of pattern recognition receptors (PRRs) due to their resemblance to infectious pathogens, thus mobilizing both adaptive and innate anti-viral mechanisms[7]. As a result, RNA vaccines induce systemic elevation of pro-inflammatory cytokines and dose-dependent, transient systemic reactions such as fever and chills[1–6,8,9]. These adverse events have been observed irrespective of administration route (intravenous (i.v.) or intramuscular delivery), formulation (liposomes or lipid nanoparticles (LNPs)) or RNA modifications (unmodified uridine or N1-methyl-pseudouridine, which reduces activation of Toll-like receptors 7 and 8 (refs. [10,11])).

In contrast to humans, C57BL/6 and Balb/c mice are remarkably tolerant to RNA vaccines and only display limited systemic cytokine release following i.v. administration of a liposomal vaccine containing unmodified RNA (RNA-LPX)[1,12]. Even at doses of RNA (50 µg) that are well tolerated in mice, patients exhibit transient mild-to-moderate flu-like symptoms that constrain dose exploration to a narrow range and possibly limit optimal T cell responses[2,4,5]. Given the obvious size differences, this means that RNA-LPX doses that trigger potent systemic inflammatory responses in humans are more than 1,000-fold lower than in inbred laboratory mice[2]. Similar observations have been made with other pro-inflammatory stimuli, creating a notable discrepancy in the dose needed to induce biological and toxicological responses in different species[1,13,14]. The mechanisms underlying these dramatic differences have remained largely unknown.

We investigated the ability of lipid-formulated RNA vaccines to trigger innate immunity. We uncovered the key role of IL-1 in triggering the release of other pro-inflammatory cytokines associated with cytokine release syndrome (CRS), with humans being markedly more sensitive than mice. Unlike humans, mice preferentially upregulated anti-inflammatory IL-1ra relative to IL-1, protecting them from uncontrolled systemic inflammation. Surprisingly, the reactogenicity of RNA vaccines was not necessarily due to the TLR7/8 agonism, as IL-1 release was observed using vaccines containing N1-methyl-pseudouridine-modified RNA (modRNA). Instead, the lipid components used to formulate these vaccines substituted for unmodified RNA in eliciting the IL-1 response.

RNA-LPX activates NLRP3 in monocytes. To identify the factors that contribute to sensitivity to innate immune stimuli, we first studied the unmodified RNA-LPX cancer vaccine, which encodes inherent TLR7/8 agonist activity[1,12]. Following RNA-LPX challenge on human peripheral blood mononuclear cells (PBMCs), a broad range of cytokines was detected in both total PBMCs and $CD14^+$ monocytes; a notable reduction in cytokine secretion was seen in CD14-depleted PBMCs, indicating that the RNA-LPX-induced cytokine response was dependent on monocytes (Fig. 1a,b and Extended Data Fig. 1a,b). The production of IL-1β prompted us to ask if RNA-LPX activated the inflammasome pathway. Cotreatment of primary human monocytes with the NLRP3 inhibitor MCC950, the gasdermin D inhibitor necrosulfonamide or the pan-caspase inhibitor zVAD-FMK abolished the release of RNA-LPX-induced IL-1β (Fig. 1c,d,e), indicating that RNA-LPX-induced, monocyte-derived IL-1β release was dependent, as expected, on inflammasome and caspase activity.

Optimal activation of the canonical NLRP3 inflammasome requires two signals[15,16]. We reasoned that synthesis of pro-IL-1β (signal 1) was primed by TLR7/8 recognition of unmodified RNA, while NLRP3 inflammasome activation (signal 2) was triggered by the liposomes themselves. Indeed, modifying the RNA by substituting

[1]Genentech, South San Francisco, CA, USA. [2]BioNTech SE, Mainz, Germany. ✉e-mail: mellman.ira@gene.com

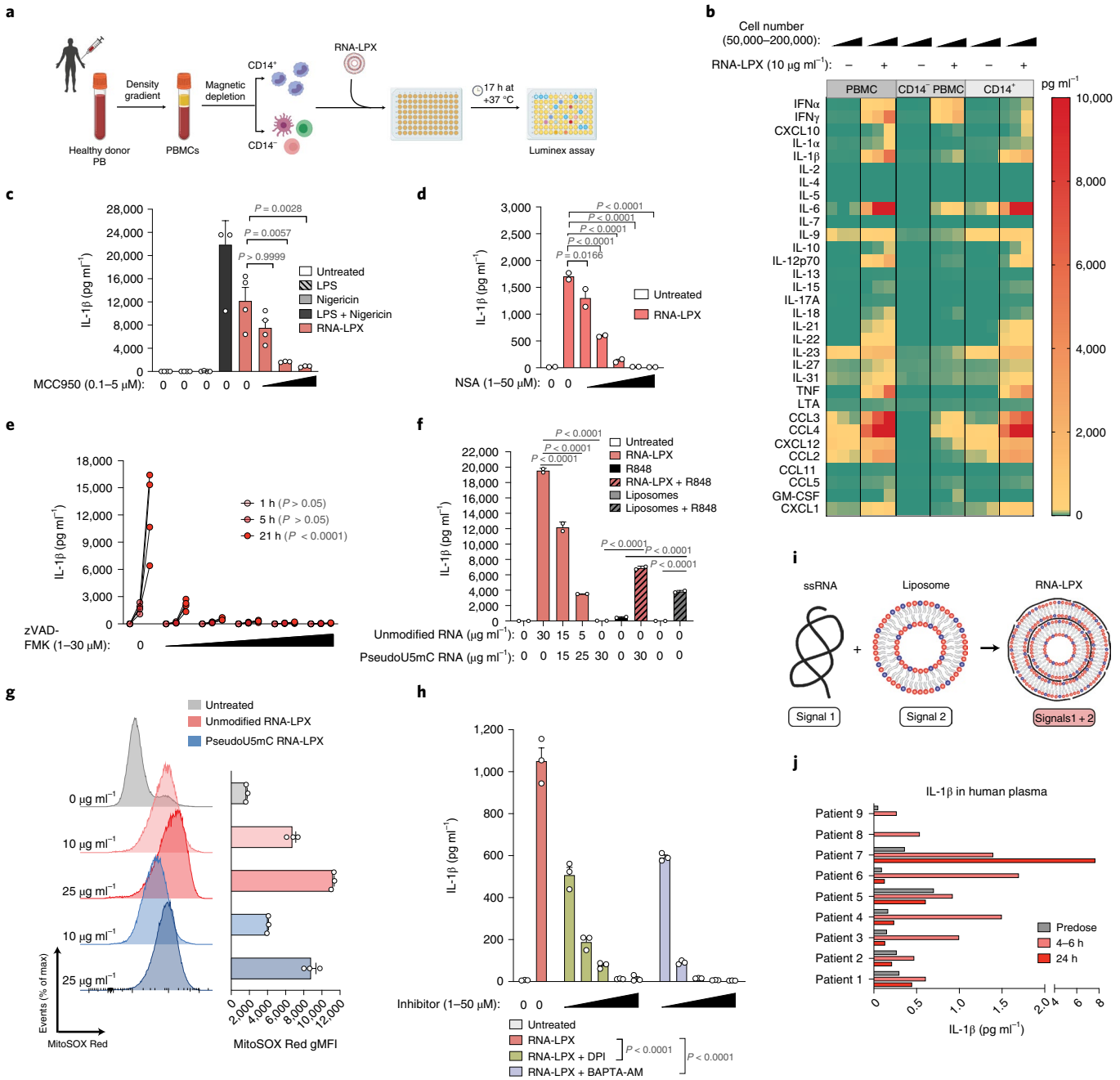

Fig. 1 | RNA-LPX induces inflammasome activation and IL-1β release in human monocytes. a,**b**, Schematic of the assay (**a**) and heatmap of RNA-LPX-induced cytokine secretion in vitro (**b**). **c**,**d**,**e**, IL-1β release from purified CD14+ monocytes in the presence of RNA-LPX and MCC950 (**c**), necrosulfonamide (NSA) (**d**) or zVAD-FMK (**e**). **f**, IL-1β release following treatment with unmodified and/or pseudoU5mC-modified RNA-LPX, and/or with R848. **g**,**h**, RNA-LPX-induced mitochondrial ROS production (**g**) or IL-1β secretion following pretreatment with DPI or BAPTA-AM (**h**). **i**, Proposed mechanism-of-action for RNA-LPX-induced inflammasome activation. **j**, Plasma IL-1β levels before and after RNA-LPX in patients ($n = 9$). The data are representative of at least three independent experiments with biologically independent samples (**b**–**h**). Data are presented as mean ± s.e.m.; $n = 4$ (**c** and **e**), $n = 3$ (**b**,**g** and **h**) or $n = 2$ (**d** and **f**). Cytokines were measured with Luminex (**b**–**h**) or with Simoa assay (**j**). Significance was determined using one-way ANOVA and Dunnett's multiple comparisons test (**c**,**d** and **h**), two-way repeated measures ANOVA and Dunnett's multiple comparisons test (**e**) or one-way ANOVA and Sidak's multiple comparisons test (**f**). gMFI, geometric mean fluorescence intensity; PB, peripheral blood.

uridine with pseudouridine and cytosine with 5-methyl-cytosine (pseudoU5mC) which renders the RNA poorly recognizable by TLR7/8 (ref. [10]) or administration of RNA-free liposomes (loss of signal 1) diminished the release of IL-1β (Fig. 1f). Similarly, the TLR7/8 agonist R848 alone failed to elicit IL-1β, while adding R848 with empty liposomes or pseudoU5mC-modified RNA-LPX resulted in readily detectable but lower IL-1β release compared with unmodified RNA-LPX (Fig. 1f).

Both unmodified and modified RNA-LPX also induced a robust generation of mitochondrial reactive oxygen species (ROS) in human monocytes (Fig. 1g). Notably, inhibition of mitochondrial ROS production using diphenyleneiodonium (DPI) or blockade of

intracellular Ca^{2+} elevation using cell-permeable calcium chelator BAPTA-AM drastically reduced RNA-LPX-induced IL-1β release (Fig. 1h). This suggests that cationic liposomes (composed of the broadly used lipids DOTMA and DOPE) provide signal 2 by inducing mitochondrial ROS-mediated calcium influx[17], possibly secondary to transient disruption of endosomal or plasma membranes[18]. The RNA-LPX complex can thus provide both signals 1 and 2 (Fig. 1i) which are required for efficient NLRP3 activation and IL-1β release from human monocytes in culture.

RNA-LPX induces IL-1 release in vivo. To determine if the in vitro findings were relevant to in vivo observations, we analyzed pre- and post-treatment plasma levels of IL-1β in a cohort of nine patients with cancer receiving RNA-LPX (autogene cevumeran) in a phase 1b study (NCT03289962). Following i.v. bolus injection of 25 μg of RNA-LPX, increase in circulating IL-1β was detected in 9 out of 9 patients to varying degrees, peaking at 4–6 h (Fig. 1j). In C57BL/6 mice, i.v. injection of RNA-LPX was also found to induce an elevation in the circulation of both IL-1β and IL-1α (Extended Data Fig. 2a,b). Although IL-1β expression was mainly observed in splenic $Ly6C^{lo}$ monocytes and neutrophils in the injected mice (Extended Data Fig. 2c,d,g), IL-1α was produced by $Ly6C^{hi}$ monocytes and red pulp macrophages (Extended Data Fig. 2e,f,g). Thus, both humans and mice upregulate IL-1 expression in monocyte/macrophage-lineage cells following RNA-LPX challenge.

IL-1α and IL-1β are important mediators of inflammatory responses well known to induce a MyD88-dependent signaling cascade upon binding to IL-1 receptor type 1 (IL-1R1)[19,20]. We next investigated the functional hierarchy of IL-1 cytokines in the context of innate immune stimulation (Fig. 2a). In the presence of IL-1β neutralizing antibodies, the RNA-LPX-induced cytokine secretion by human PBMCs was completely or almost completely blocked (Fig. 2b,c). Thus, the expression and release of IL-1β appeared to control the induction of most pro-inflammatory cytokines, including TNF and IL-6 (Fig. 2c). TNF blockade did not significantly reduce IL-6 release, nor did an anti-IL-6 antibody reduce TNF release (Extended Data Fig. 3a), indicating that cytokine release secondary to innate stimulation by RNA-LPX was mechanistically distinct from the CRS cascade initiated by T cell-activating therapies, where anti-TNF and anti-IL-6 are both effective inhibitors of the cytokine response[21–23]. Of note, out of all of the cytokines and chemokines screened, only CCL5 (also known as RANTES) was upregulated following IL-1β blockade, suggesting that IL-1 signaling negatively regulates the induction of CCL5 (Fig. 2b,c).

Systemic cytokine levels following RNA-LPX treatment were also significantly attenuated in IL-1R1-deficient ($Il1r1^{-/-}$) mice as compared with wildtype mice both in vitro (Extended Data Fig. 3b,c) and in vivo (Fig. 2d,e). Consistent with our human data, in mice RNA-LPX-induced IL-1R1 signaling occurred upstream of IL-6 and TNF release, although the effect on TNF was less pronounced in the knockouts (Fig. 2e and Extended Data Fig. 3c). In contrast to $Il1r1^{-/-}$ mice, RNA-LPX administration did not result in a decreased serum cytokine response in NLRP3-deficient ($Nlrp3^{-/-}$) mice (Extended Data Fig. 4a,b) or in gasdermin D-deficient ($Gsdmd^{-/-}$) mice (Extended Data Fig. 4c,d). This finding can be understood from the fact that in mice, RNA-LPX also elicited the release of ~40-fold more IL-1α as compared with IL-1β (Extended Data Fig. 2b). IL-1α can activate IL-1R1 signaling independently of inflammasomes[20], but nevertheless still controls the systemic cytokine response in mice (as opposed to IL-1β in human cells). Taken together, IL-1 appears to have a critical determinative role in amplifying cytokine responses initiated by innate immune stimuli both in humans and in mice.

IL-1 induction hierarchy varies between species. Due to its highly pro-inflammatory potential, the IL-1 signaling pathway is tightly regulated by soluble IL-1R1 as well as soluble and membrane forms of IL-1 receptor 2 (IL-1R2), each of which act as ligand traps or 'decoys'[20]. Additionally, IL-1ra, a secreted anti-inflammatory cytokine, competes with active IL-1 and blocks binding to their common activating receptor, IL-1R1 (refs. [24–26]). We first asked if IL-1ra production might play a role in modulating the activity of IL-1 induced by RNA-LPX by determining the amounts of IL-1α, IL-1β and IL-1ra released from human PBMCs. At lower dose levels of RNA-LPX (<2 μg ml^{-1}), IL-1β and IL-1ra were released in nearly equivalent amounts (Fig. 3a). However, at higher RNA-LPX doses, the release of IL-1β markedly increased (~10-fold), greatly exceeding the release of IL-1ra, which remained constant (Fig. 3a). Thus, the 'buffering capacity' of IL-1ra is likely to be overcome as the degree of innate stimulation is increased. Of note, IL-1α levels remained low at all RNA-LPX dose levels in human cells (Fig. 3a).

Since mice are much less sensitive to RNA-LPX than humans (Extended Data Fig. 5a,b), we next asked if a similar IL-1 induction hierarchy occurred in mice. In stark contrast to human cells, IL-1ra was already highly released by murine leukocytes at baseline and further increased upon RNA-LPX; induction of IL-1α and IL-1β was only observed at high dose levels (Fig. 3b). We then treated C57BL/6J mice with RNA-LPX in vivo (Fig. 3c). While treatment with RNA-LPX induced a >10-fold upregulation of IL-1β and IL-1α, serum levels of IL-1ra were similarly induced and remained in ~100-fold molar excess over IL-1β and 10-fold excess over IL-1α (Fig. 3c, left panel). Qualitatively similar results were obtained from C57BL/6J mouse spleen (Fig. 3c, right panel) and from the serum of other sub-strains of C57BL/6 and Balb/c wildtype mice regardless of vendor origin or strain (Extended Data Fig. 5c).

To compare IL-1β versus IL-1ra release in vivo, we calculated the fold induction of systemic cytokine levels in C57BL/6 mice and in the nine patients with cancer from the phase 1b study, both groups having been treated with comparable absolute amounts of RNA-LPX. As expected based on the in vitro data, human patients treated with a tolerated dose of 25 μg showed a slight increase in induction of IL-1β over IL-1ra, whereas in mice, IL-1ra was dramatically induced relative to IL-1β (Fig. 3d). Of note, rather than normalizing RNA-LPX doses per animal weight, mice were administered identical absolute amounts of RNA-LPX as human patients (25 μg per injection). These findings suggest that IL-1ra can attenuate the effect of IL-1β in humans but only at low-to-moderate doses of RNA-LPX, while the substantial induction of IL-1ra would be expected to provide a far higher degree of attenuation against increases in IL-1α/β release in mice.

We also measured the respective cytokine levels in nonhuman primate (NHP) cells, as cynomolgus macaques and rhesus macaques are often used to assess safety and immunogenicity of RNA vaccines[27]. Interestingly, robust upregulation of IL-1ra was detected at all RNA-LPX dose levels, while IL-1β concentration and monocyte frequency were found to be lower in both cynomolgus macaque and rhesus macaque PBMCs compared with human PBMCs (Extended Data Fig. 5d–f). These results suggest that similar to mice, preclinical studies in NHPs might not fully capture the inflammatory toxicities related to RNA vaccines.

IL-1ra is the primary regulator of responses to RNA-LPX. To test directly whether the high systemic levels of IL-1ra explained the marked difference in tolerability between humans and mice, we administered RNA-LPX to IL-1ra-deficient ($Il1rn^{-/-}$) mice and wildtype littermates. As observed previously, high-dose RNA-LPX (100 μg) was well tolerated in wildtype mice without any detectable adverse events. In contrast, RNA-LPX-treated $Il1rn^{-/-}$ mice rapidly developed a CRS-like phenotype characterized by pronounced hypothermia (Fig. 3e), body weight loss (Fig. 3f) and excessive systemic cytokine release (Fig. 3g). Notably, these adverse events were transient and resolved within days, similar to observations

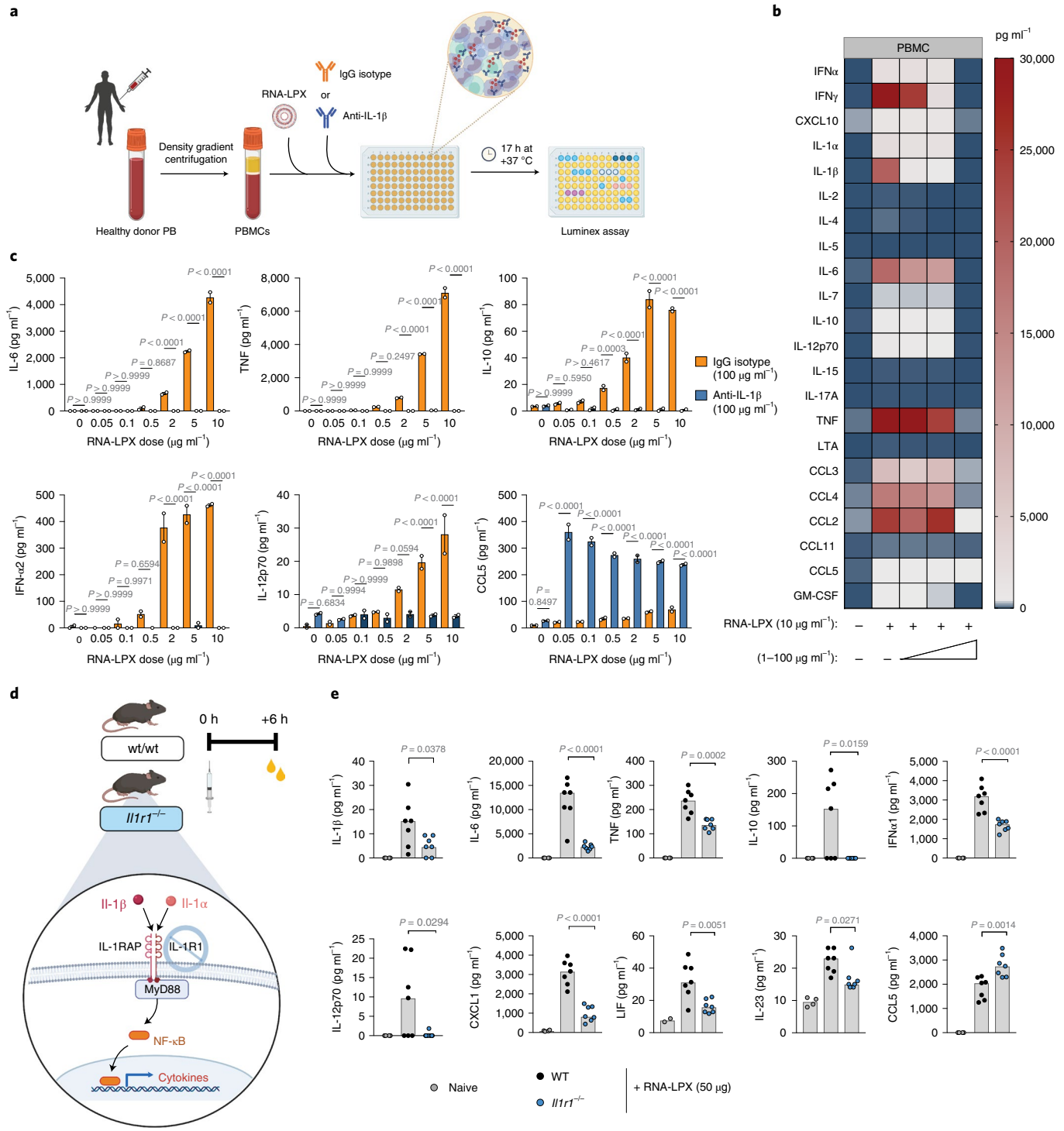

Fig. 2 | IL-1 mediates RNA-LPX-induced cytokine release. a–c, Schematic of the assay (**a**) and RNA-LPX-induced cytokines in PBMCs treated with either increasing doses of neutralizing anti-IL-1β antibodies ($n=3$) (**b**) or with a constant dose of anti-IL-1β and increasing concentrations of RNA-LPX ($n=2$) (**c**). **d**,**e**, Schematic of the experiment (**d**) and serum cytokine levels in wildtype and IL-1R1 deficient mice ($n=7$) after i.v. injection of RNA-LPX (**e**). The data are representative of at least two independent experiments with biologically independent samples (**b–e**). Cytokines were measured with Luminex (**b–e**). Significance was determined using one-way ANOVA and Sidak's multiple comparisons test (**c**) or one-way ANOVA and Dunnett's multiple comparisons test (**e**). Data are presented as median (**e**), or otherwise mean ± s.e.m. WT, wildtype.

in human patients[2,4,5]. In the absence of IL-1ra, a marked increase in a wide range of pro-inflammatory cytokines was observed in systemic circulation (Fig. 3g). In addition, *Il1rn*$^{-/-}$ mice upregulated acute phase proteins such as serum amyloid A3 (SAA3), the murine equivalent to the human C-reactive protein (Fig. 3g). These differences could only be detected following RNA-LPX administration, as no differences in systemic cytokines were observed at baseline (Extended Data Fig. 6).

As neutrophilia was detected in untreated *Il1rn*$^{-/-}$ animals (Extended Data Fig. 6a–c), we decided to test whether the increased

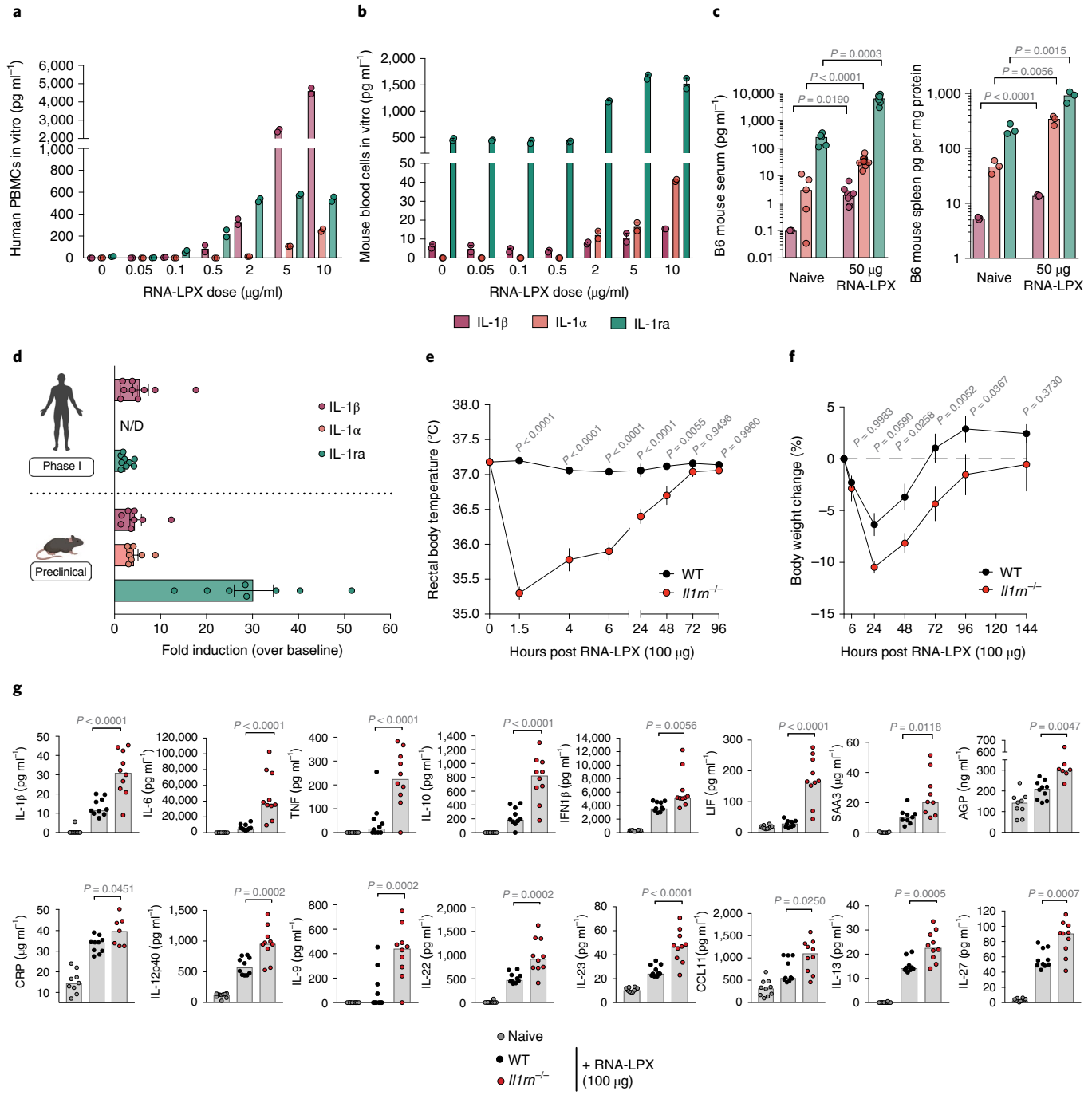

Fig. 3 | Robust upregulation of IL-1ra following RNA-LPX protects mice from IL-1-mediated adverse events in vivo. a–c, Hierarchy of IL-1 family members following overnight treatment with RNA-LPX in human PBMCs (**a**) or murine blood cells in vitro (**b**), and in C57BL/6 mice in vivo 6 h after dosing (**c**, $n = 8$, left panel and $n = 3$, right panel). **d**, Fold induction of systemic cytokines over predose levels 4–6 h after 25-μg RNA-LPX administration in patients ($n = 9$) and in wildtype mice ($n = 8$). **e–g**, Core body temperature (**e**), body weight (**f**) and serum cytokines (**g**) in wildtype and *Il1rn*$^{-/-}$ mice after i.v. administration of RNA-LPX. The data are representative of at least two independent experiments (**a–c**) or pooled from two independent experiments (**f** and **g**) with biologically independent samples; $n = 5$ (**e**,**f**) or $n = 10$ (**g**). Cytokines were measured with Luminex (**a–g**). Significance was determined using unpaired two-tailed Student's *t*-test (**c**), two-way repeated measures ANOVA and Sidak's multiple comparisons test (**e** and **f**) or one-way ANOVA and Dunnett's multiple comparisons test (**g**). Data are presented as median (**a–c** and **g**), or otherwise mean ± s.e.m. AGP, alpha 1-acid glycoprotein; CCL11, C-C motif chemokine ligand 11; CRP, C-reactive protein; LIF, Leukemia inhibitory factor; N/D, not detectable.

neutrophil count could be driving the exacerbated systemic cytokine responses. To this end, mice were pretreated with two doses of depleting anti-Ly6G antibodies before RNA-LPX administration (Extended Data Fig. 7a). Surprisingly, the depletion of Ly6G^{+} cells led to a moderate increase in RNA-LPX-induced IL-6 in *Il1rn*$^{-/-}$ mice but not in wildtype littermates (Extended Data Fig. 7b). This may be explained by an induction of cell-surface IL-1R2 on neutrophils in *Il1rn*$^{-/-}$ mice following RNA-LPX exposure (Extended Data Fig. 7c), suggesting a similar IL-1 inhibition mechanism as seen previously in humans[28].

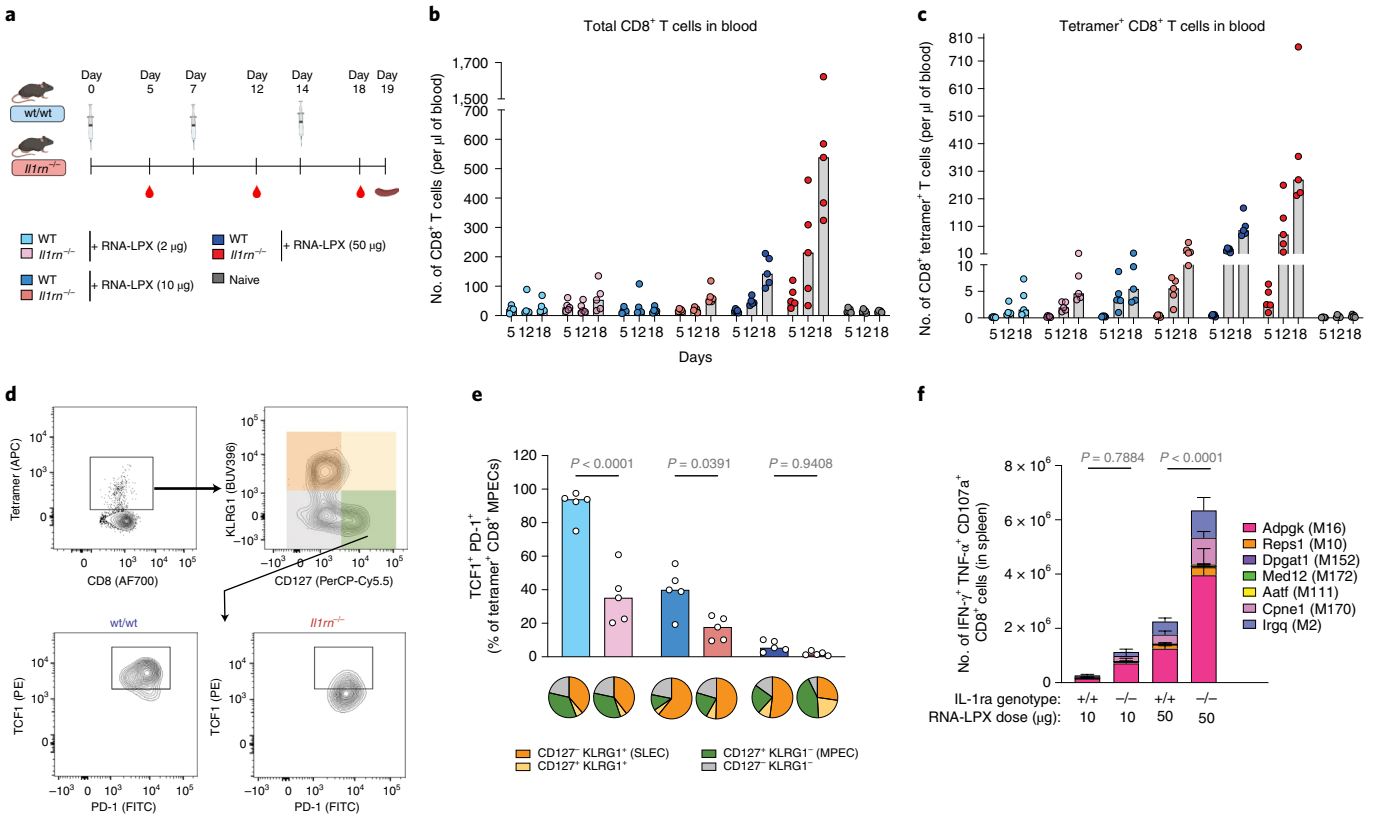

Fig. 4 | IL-1ra regulates adaptive responses to RNA-LPX. a–c, Vaccination schedule (**a**), and levels of total (**b**) and neoantigen-specific T cells (**c**) in blood of wildtype and *Il1rn*$^{-/-}$ mice ($n = 5$) following weekly i.v. injections of RNA-LPX. **d**,**e**, Gating strategy (**d**), expression pattern of CD127 and KLRG1 within tetramer$^+$ T cells (**e**, lower panel) and frequency of TCF1$^+$PD-1$^+$ T cells within CD127$^+$KLRG1$^-$tetramer$^+$ T cells (**e**, upper panel) in spleen on day 19. **f**, Intracellular cytokine expression in splenic T cells following re-stimulation with seven neoantigen-specific peptides ex vivo ($n = 5$). The data are representative of at least two independent experiments (**b**–**f**). Significance was determined using one-way ANOVA and Dunnett's multiple comparisons test (**e**) or two-way ANOVA and Tukey's multiple comparisons test (**f**). Data are presented as median (**e**), or otherwise mean ± s.e.m. APC, allophycocyanin; PE, phycoerythrin; SLEC, short-lived effector cell; MPEC, memory precursor effector cell; TCF1, T cell factor 1; PD-1, programmed cell death protein 1.

To fully assess the importance of the myeloid compartment on the magnitude of systemic inflammatory response, we also pretreated wildtype and *Il1rn*$^{-/-}$ mice with nine daily doses of murine FMS-like tyrosine kinase 3 ligand (Flt3L) (Extended Data Fig. 7d), which induces expansion of splenic macrophages, monocytes, dendritic cells and neutrophils[29]. Following i.v. administration of 50 µg of RNA-LPX, a markedly enhanced systemic cytokine response was observed in Flt3L-pretreated *Il1rn*$^{-/-}$ mice (Extended Data Fig. 7e), leading to lethal inflammation in 66% of these animals by 24 h post-vaccination. Interestingly, similar toxicities were not observed in Flt3L-pretreated wildtype animals, likely due to augmented induction of IL-1ra (Extended Data Fig. 7e). Altogether, these results show that endogenous IL-1ra can suppress IL-1-induced adverse events in mice and explain their tolerability to high doses of RNA-LPX.

In addition to contributing to the reactogenicity of the vaccine, IL-1 has been reported to serve as an innate instructor of adaptive immunity[30]. To study the role of IL-1 in vaccine-induced T cell responses, we injected *Il1rn*$^{-/-}$ and wildtype littermate mice with weekly doses of 2 µg, 10 µg or 50 µg of RNA-LPX vaccines encoding for seven previously characterized MC38 tumor neoantigens[31] (Fig. 4a). While a dose-dependent expansion in total and neoantigen-specific T cells in blood was observed in both genotypes over time, markedly higher T cell counts were recorded in vaccinated IL-1ra-deficient mice compared with wildtype mice (Fig. 4b,c). Alternatively, lower doses or fewer vaccinations of RNA-LPX were required to induce comparable T cell responses in the absence of IL-1ra (Fig. 4c). To further assess the quality of the vaccine-induced T cells, we collected spleens 7 d after the final immunization for flow cytometric characterization. Analysis of T cell differentiation markers suggested that neoantigen-specific T cells exhibited a memory precursor effector cell (that is, CD127$^+$ KLRG1$^-$) phenotype in the absence of IL-1ra, while a higher proportion of vaccine-induced T cells in wildtype mice were short-lived effector cells (that is CD127$^-$ KLRG1$^+$) following three vaccinations with 10 µg or 50 µg of RNA-LPX (Fig. 4d,e). We also observed a significant down regulation of TCF1 in splenic tetramer$^+$ memory precursor effector cells in *Il1rn*$^{-/-}$ mice on day 19 (Fig. 4e), consistent with the robust T cell expansion in blood on day 18 (Fig. 4b,c) and enhanced polyfunctionality in spleen following peptide re-stimulation on day 19 (Fig. 4f). Thus, our findings indicate that even if limited by the antigen dose, unmodified RNA vaccines represent an effective approach to induce antigen-specific T cell responses when sufficient innate stimulus is provided, as suggested by clinical data[1,2,4,5].

IL-1ra controls systemic responses to inflammatory stimuli. Given that excessive systemic inflammatory responses are commonly observed in human pathologies ranging from sepsis to viral infections, we asked if the regulatory role of IL-1ra could be generalized to other types of innate immune stimulation. TLR and STING agonists induced bone-marrow-derived myeloid cell cultures to secrete variable but notable levels of IL-1ra (Fig. 5a,b). In each case, IL-1ra induction was far greater than that seen for either IL-1α or IL-1β. Next, we injected a single systemic dose of lipopolysaccharide

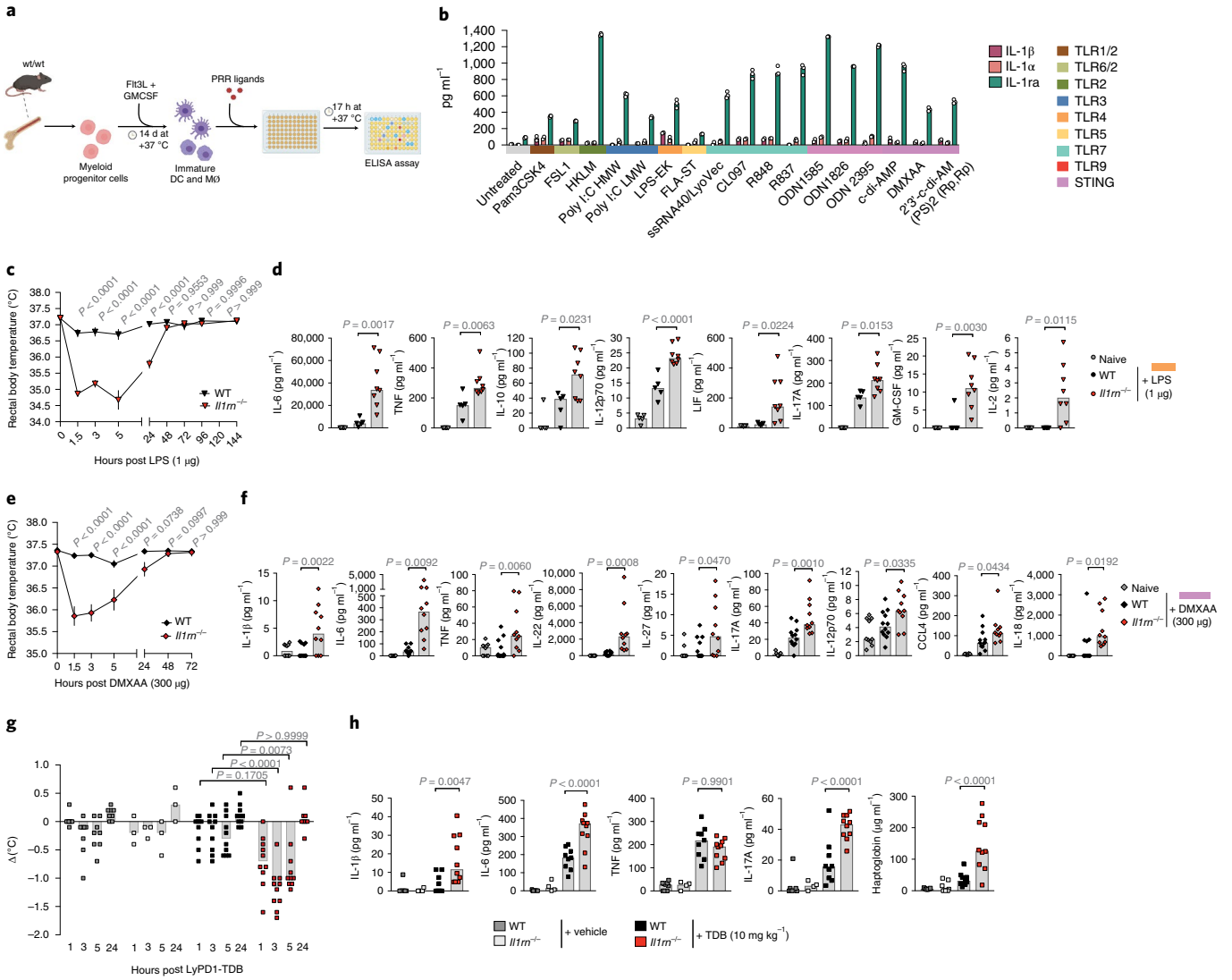

Fig. 5 | IL-1ra regulates the response to and degree of sensitivity to innate and adaptive immune stimuli. a,**b**, Schematic of the assay (**a**) and secretion of IL-1α, IL-1β and IL-1ra from murine bone-marrow-derived DC/Mϕ cultures following treatment with different PRR ligands in vitro (**b**). **c**,**d**, Core body temperature (**c**) and serum proteins (**d**) in wildtype and *Il1rn*$^{-/-}$ mice after systemic administration of LPS ($n = 8$). **e**, **f**, Core body temperature (**e**) and serum proteins (**f**) in wildtype and *Il1rn*−/− mice after systemic administration of DMXAA ($n = 10$). **g**,**h**, Changes in core body temperature (**g**) and serum cytokines (**h**) in ID8/LyPD1 tumor-bearing mice ($n = 10$) after i.v. administration of anti-CD3/anti-LyPD1 TDB. The data are representative of three independent experiments with biologically independent samples (**b**) or pooled from two independent experiments with biologically independent samples (**c**–**h**). Cytokines were measured with Luminex (**b**–**h**). Significance was determined using two-way repeated measures ANOVA and Sidak's multiple comparisons test (**c**,**e** and **g**) or one-way ANOVA and Dunnett's multiple comparisons test (**d**,**f** and **h**). Data are presented as median (**d**,**f** and **h**), or otherwise mean ± s.e.m. DC, dendritic cell ; Mϕ, macrophage.

(LPS,TLR4 agonist), ODN1826 (TLR9 agonist), heat-killed *Listeria monocytogenes* (HKLM, a TLR2 agonist) or DMXAA (STING agonist) into wildtype or *Il1rn*$^{-/-}$ mice (Fig. 5c–f and Extended Data Fig. 8). As observed with RNA-LPX, increased sensitivity and self-limited hypothermia were observed in IL-1ra-deficient mice treated with these innate pro-inflammatory ligands (Fig. 5c,e and Extended Data Fig. 8a,c). Moreover, significant elevations in a range of serum cytokines were observed in *Il1rn*$^{-/-}$ mice (Fig. 5d,f and Extended Data Fig. 8b,d). These results indicate that high endogenous levels of IL-1ra can protect wildtype mice from immune dysregulation and uncontrolled systemic inflammation triggered by IL-1 for a range of innate stimulatory agents.

Lastly, T cell-based immunotherapies such as chimeric antigen receptor (CAR)T cells and tumor-directed/CD3-bispecific antibodies (TDBs) can also cause clinical CRS in human patients[21–23,32]. Instead of inducing a direct, primary release of IL-1β by innate stimuli (such as RNA-LPX), these immunotherapies have been shown to trigger a secondary induction of IL-1β, driven by activation of T cells[21–23]. We asked if IL-1β released secondary to initial stimuli would contribute to the development of CRS in *Il1rn*$^{-/-}$ mice bearing ID8 tumors expressing the surface antigen LyPD1. Following administration of an anti-LyPD1/CD3 TDB, upregulation of IL-1β expression in monocytes and macrophages was observed in vivo (Extended Data Fig. 9). The systemic release of IL-1β instigated a rapid decrease in core body temperature in TDB-treated *Il1rn*$^{-/-}$ mice (Fig. 5g), accompanied by elevated serum concentrations of IL-6 and IL-17A (Fig. 5h). Of note, the serum concentrations of TNF were comparable between genotypes (Fig. 5h). This further suggests that while T cells provide the initial trigger for CRS, T cell-derived TNF probably serves to activate monocytes and macrophages to

release IL-1β, which was then directly responsible for the transient systemic response to TDBs in vivo. Importantly, these data suggest that induction of IL-6, which has been shown to be an important mediator of CRS toxicities related to T cell-targeting therapies[21–23], can occur downstream of IL-1β.

***Il1rn*$^{-/-}$ mice adapt to excessive IL-1 via shedding of IL-1R1.** Despite lacking the master negative regulator of IL-1, IL-1ra deficient mice should still possess the other presumed negative regulators of IL-1 activity. Indeed, increase in soluble IL-1R1 was observed in the serum of *Il1rn*$^{-/-}$ mice following stimulation with innate ligands (Fig. 6a), concomitant with reduction in cell-surface expression of IL-1R1 in vivo (Fig. 6b). This loss of membrane-bound IL-1R1 can decrease signaling and provide a soluble systemic IL-1α/β sink in the absence of IL-1ra. Interestingly, blockade of IL-1 signaling with a recombinant IL-1R1-Fc prevented the loss of cell-surface IL-1R1 in *Il1rn*$^{-/-}$ blood cells ex vivo (Fig. 6c), suggesting that the shedding of IL-1R1 only occurs following excessive IL-1 signaling (that is, in the absence of IL-1ra). In contrast to IL-1R1, the serum concentrations of decoy receptor IL-1R2 were only modestly increased over high baseline levels following stimulation (Fig. 6d), suggesting that shedding of IL-1R1 was the primary resistance mechanism by which *Il1rn*$^{-/-}$ mice adapt to excessive IL-1 signaling (Fig. 6e). However, these changes were secondary and only upregulated in the absence of IL-1ra, confirming that IL-1ra is the key suppressor of PRR-induced reactogenicity in wildtype mice.

Ionizable lipids in modRNA-LNP induce the release of IL-1. Our data with RNA-LPX indicated that both TLR7/8 agonistic function of the RNA and liposomes were required for production of IL-1, which mediated reactogenicity and immunogenicity of the vaccine. However, RNA vaccines against COVID-19 (mRNA-1273 by Moderna and BNT162b2 by BioNTech/Pfizer)—which use modRNA with a greatly reduced innate immunostimulatory activity—still elicit systemic adverse events in patients following initial intramuscular administration[3,6,8,9]. Instead of cationic liposomes, these vaccines are formulated in LNPs which contain ionizable lipids to provide structural stability and presumably enable endosomal escape[7,33]. While LNPs have been observed to have intrinsic adjuvant activity, demonstrated by the impressive antibody and T cell responses following vaccination[3,6,8,9], the exact mechanism of by which such vaccines elicit innate immunity has not been previously characterized.

To test whether these particles could induce release of different IL-1 family members, we generated modRNA-LNPs formulated with two different ionizable lipids: MC3 (commonly used for short interfering RNA (siRNA)-LNP delivery[33]) or SM-102 (used in the Moderna COVID-19 vaccine[8,33]) (Fig. 7a). Consistent with our findings with RNA-LPX, we observed a marked increase in IL-1β from human PBMCs with either modRNA-LNP formulation, while the levels of IL-1α and IL-1ra remained low (Fig. 7b). LNPs formulated with SM-102 lipids were potent activators of the inflammasome pathway, indicated by the fact that robust IL-1β release was detected with either modRNA-LNP(SM-102) or empty LNP(SM-102) (Fig. 7c). Cotreatment with R848 and empty LNP(SM-102) further increased the IL-1β levels (Fig. 7c). In contrast, modRNA-LNP(MC3) was far less potent at stimulating IL-1β release, and even addition of a strong TLR7/8 agonist, R848, to LNP(MC3) could not fully rescue IL-1β release (Fig. 7c). These results suggest that ionizable lipids in different LNP formulations can play different, yet important, roles in inflammasome activation by providing either signal 2 (MC3) or signals 1 and 2 (SM-102).

To further study the relative contributions of RNA and lipids, we used modRNA to make RNA-LPX particles (modRNA-LPX) and compared their cytokine induction profile with RNA-LPX and modRNA-LNP(SM-102) (Fig. 7d). As shown previously (Fig. 1), unmodified RNA-LPX induced a robust cytokine release, whereas modRNA-LPX failed to induce IL-1β or any of its downstream cytokines (Fig. 7e). In contrast, potent cytokine release was detected with modRNA-LNP(SM-102), resulting in a similar cytokine induction profile as with RNA-LPX (Fig. 7e). These findings suggest that the reactogenicity of modified RNA is context-dependent: modRNA can be nonimmunostimulatory when formulated in liposomes (LPX), induce weak immunostimulation when formulated in LNP(MC3) or initiate a potent innate response when formulated in LNP(SM-102).

Discussion

The evolution of the innate immune system for any species has in large part been shaped by microbe-exerted selection pressure for that species. While this has led to differences in distribution, sensitivity and ligand specificity of PRRs, it has also resulted in diverging evolutionary strategies for resistance and tolerance between humans and mice[34]. Relative to human immune responses, mice have been found to be extremely tolerant to different inflammatory stimuli[13,14,34], such as bacterial lipopolysaccharides, but also RNA-LPX vaccines[1,12]. In this study, we demonstrated that vaccine-induced systemic inflammatory responses are driven by IL-1 and antagonized by endogenous IL-1ra, and that these findings can be generalized to other forms of innate immune stimulation. Interestingly, clinical use of recombinant IL-1ra (anakinra) may be effective for the treatment of auto-immune-related macrophage activation syndrome and severe forms of COVID-19, suggesting that IL-1R1 signaling can contribute to the early cytokine amplification following infection[35–37]. In line with these reports, we observed that administration of a virus-like nanoparticulate vaccine, RNA-LPX, leads to a robust upregulation of IL-1ra in wildtype B6 mice and confers resistance to adverse events, while *Il1rn*$^{-/-}$ mice exhibited a phenotype reminiscent of human CRS following innate immune challenge. These results suggest that endogenous IL-1ra has a crucial role in controlling innate immune responses to pathogens, as shown for *Mycobacterium tuberculosis*[38]. In addition, reduced sensitivity of mouse blood cells to RNA-LPX could be partially explained by the lower frequency of monocytes in mice when compared with humans, as we and others have identified monocytes as the crucial cell population secreting IL-1β and IL-6 following stimulation[21,23]. Accordingly, the absence of granulocytes in these cellular assays did not produce any changes in IL-1β release. Our studies with NHP PBMCs also suggest that NHPs resemble mice more than humans with respect to their monocyte frequencies and IL-1ra induction profile. Of note, NHPs and humans exhibit notable evolutionary differences in response to innate stimuli, and TLR7/8 agonists have been reported to be poor inducers of pro-IL-1β in NHP cells[39].

Furthermore, our studies revealed that not only the direct TLR7/8-mediated sensing of the nucleic acid component, but also the physiochemical and possibly lytic properties of the vaccine lipid particles themselves, determine the cytokine induction profile of lipid-formulated RNA vaccines. Our data indicate that the immunostimulatory activity of the modRNA is highly dependent on the lipid formulation; modRNA formulated in LPX is nonimmunostimulatory and has been shown to induce tolerance[40], while formulation in LNP(SM-102) leads to potent innate response, consistent with the reactogenicity and immunogenicity observed in mRNA-1273-vaccinated individuals[8]. Although modRNA poorly activates TLR7/8, it can have residual innate agonist properties, possibly resulting from double-stranded RNA contamination produced during in vitro transcription, remaining uncapped messenger RNA or mRNA tertiary structures, any of which can be a source of signal 1 by activating various endosomal (TLR3) and cytosolic receptors (for example, RIG-I, MDA-5). However, we also observed that empty LNP(SM-102) particles without RNA were sufficient for IL-1β release in vitro, suggesting that the lipids alone can provide

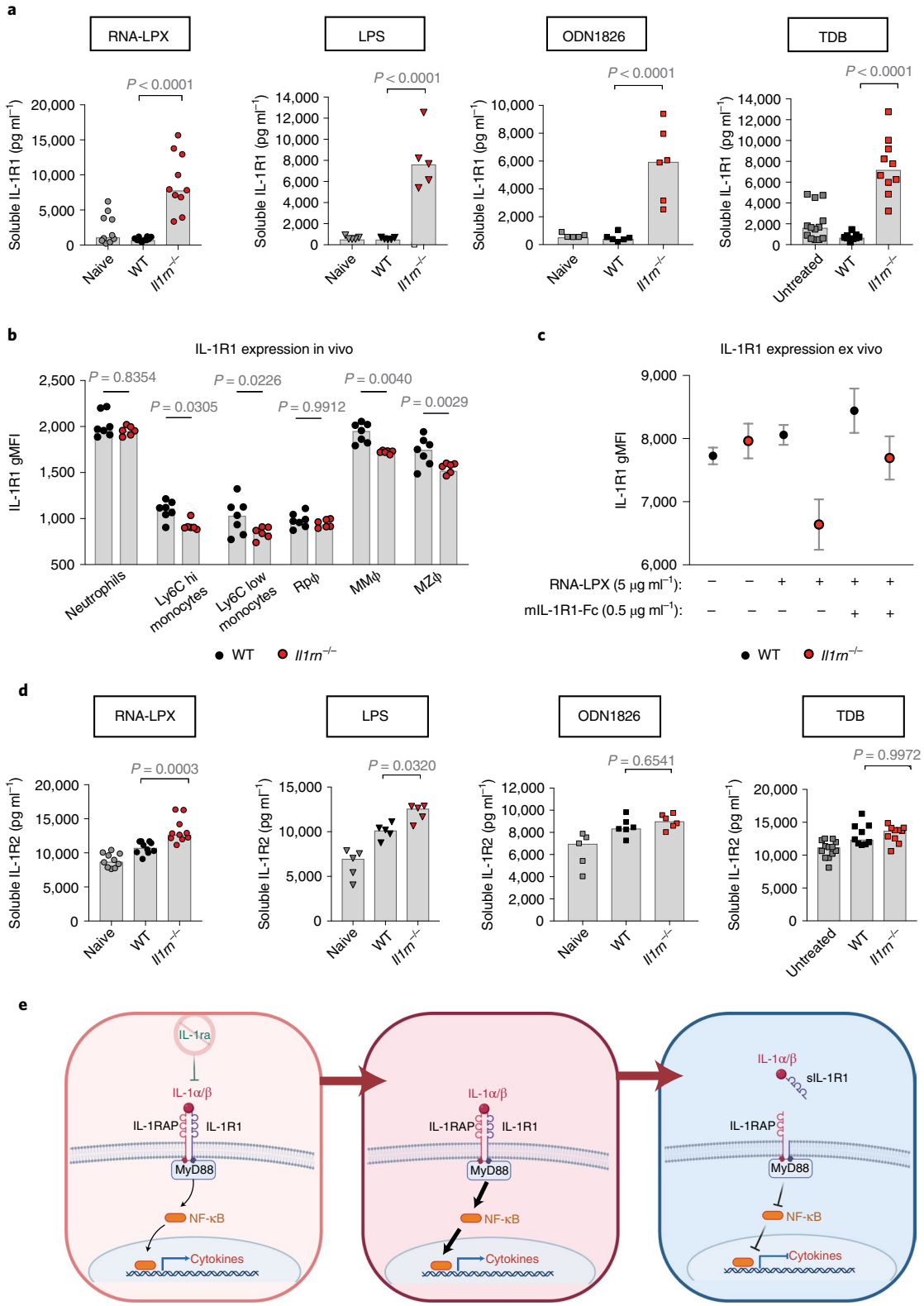

Fig. 6 | Increased shedding of IL-1R1 is a compensatory inhibition mechanism to prevent excessive IL-1 signaling in *Il1rn*$^{-/-}$ mice. a, Soluble IL-1R1 in the serum of wildtype and *Il1rn*$^{-/-}$ mice after i.v. administration of RNA-LPX ($n=10$), LPS ($n=5$), ODN1826 ($n=6$) or anti-CD3/anti-LyPD1 TDB ($n=10$). **b**, gMFI of IL-1R1 expression in the spleen of *Il1rn*$^{-/-}$ ($n=6$) and wildtype littermate mice ($n=7$) 24 h post-RNA-LPX administration. **c**, gMFI of IL-1R1 on wildtype and *Ilrn*$^{-/-}$ ACK-treated blood cells following treatment with RNA-LPX with or without recombinant murine IL-1R1-Fc ex vivo. **d**, Soluble IL-1R2 in the serum of wildtype and *Il1rn*$^{-/-}$ mice after i.v. administration of RNA-LPX ($n=10$), LPS ($n=5$), ODN1826 ($n=6$) or anti-CD3/anti-LyPD1 TDB ($n=10$). **e**, Proposed mechanism-of-action for IL-1R1 shedding following excessive IL-1 signaling in *Il1rn*$^{-/-}$ mice. Significance was determined using one-way ANOVA and Dunnett's multiple comparisons test. ACK, Ammonium-Chloride-Potassium; Rpϕ, red pulp macrophage; MMϕ, marginal metallophilic macrophage; MZϕ, marginal zone macrophage. Data are presented as mean ± s.e.m. (**c**), or otherwise median.

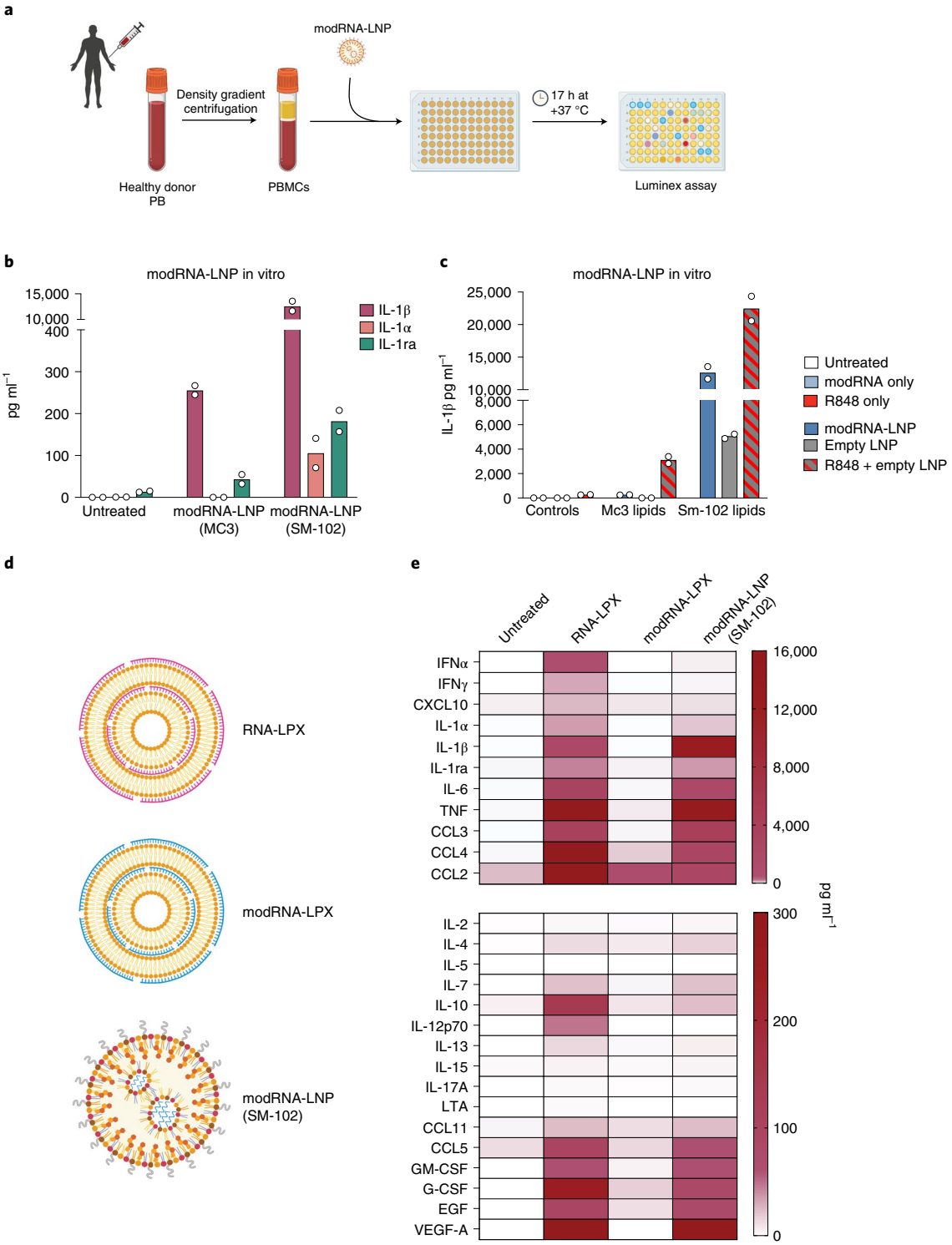

Fig. 7 | modRNA-LNP induces IL-1β in human PBMCs in vitro. a,**b**, Schematic of the assay (**a**) and secretion of IL-1β, IL-1α and IL-1ra from human PBMCs following treatment with N1-methyl-pseudouridine (N1psU)-modified RNA-LNP (modRNA-LNP, formulated with either MC3 or SM-102 lipids) in vitro (**b**). **c**, IL-1β release following treatment with either modRNA-LNP or empty LNPs with or without R848. **d**, Schematic of the different lipid-formulated RNA vaccines. **e**, Cytokine release from PBMCs treated with unmodified RNA-LPX, N1psU-modified RNA-LPX (modRNA-LPX) or modRNA-LNP (formulated with SM-102 lipids). The data are representative of two independent experiments with biologically independent samples. Data are presented as median.

both signals 1 and 2 for inflammasome activation. While we did not investigate the source of signal 1 in this context, it could be derived from direct activation of PRRs by the lipids themselves[41–43], from the release of damage-associated molecular patterns following cell damage caused by LNPs[44] or from the direct activation of caspase-11 (ref. [45]). Future work will determine how these factors will influence the overall immunogenicity profile of LNP-based particles and whether such responses could be altered by the use of alternative

lipid structures. Importantly, such optimizations will be crucial for the entire field of oligonucleotide therapeutics, where—unlike for adjuvanted vaccines—the induction of the innate immune cascade mediated by IL-1β would be undesirable (for example, LNP-based therapeutics delivering siRNA, antisense oligonucleotides or immune-tolerance-inducing mRNA).

In summary, our findings indicate that that IL-1ra-deficient mice can better predict patient responses to innate immune challenges (such as RNA vaccines) and provide a useful tool to evaluate both the sensitivity to pathogens and tolerability to treatment-related inflammatory toxicities in vivo. Moreover, the observed interspecies differences suggest that evolution has shaped and re-wired how positive and negative regulators of IL-1R1 signaling are released in the context of innate immune stimulation, and that these factors determine the magnitude of systemic responses to RNA vaccines in mice, NHPs and humans.

Online content

Any methods, additional references, Nature Research reporting summaries, source data, extended data, supplementary information, acknowledgements, peer review information; details of author contributions and competing interests; and statements of data and code availability are available at https://doi.org/10.1038/s41590-022-01160-y.

Received: 23 November 2021; Accepted: 15 February 2022;
Published online: 24 March 2022

References

1. Kranz, L. M. et al. Systemic RNA delivery to dendritic cells exploits antiviral defence for cancer immunotherapy. *Nature* **534**, 396–401 (2016).
2. Sahin, U. et al. An RNA vaccine drives immunity in checkpoint-inhibitor-treated melanoma. *Nature* **585**, 107–112 (2020).
3. Sahin, U. et al. COVID-19 vaccine BNT162b1 elicits human antibody and TH1 T-cell responses. *Nature* **586**, 594–599 (2020).
4. Braiteh, F. et al. Abstract CT169: A phase Ia study to evaluate RO7198457, an individualized Neoantigen Specific immunoTherapy (iNeST), in patients with locally advanced or metastatic solid tumors. *Cancer Res.* **80** (Suppl.), abstr. CT169 (2020).
5. Lopez, J. S. et al. Abstract CT301: A phase Ib study to evaluate RO7198457, an individualized Neoantigen Specific immunoTherapy (iNeST), in combination with atezolizumab in patients with locally advanced or metastatic solid tumors. *Cancer Res.* **80** (Suppl.), abstr. CT301 (2020).
6. Mulligan, M. J. et al. Phase I/II study of COVID-19 RNA vaccine BNT162b1 in adults. *Nature* **586**, 589–593 (2020).
7. Pardi, N., Hogan, M. J., Porter, F. W. & Weissman, D. mRNA vaccines—a new era in vaccinology. *Nat. Rev. Drug Discov.* **17**, 261–279 (2018).
8. Jackson, L. A. et al. An mRNA vaccine against SARS-CoV-2—preliminary report. *N. Engl. J. Med.* **383**, 1920–1931 (2020).
9. Cafri, G. et al. mRNA vaccine–induced neoantigen-specific T cell immunity in patients with gastrointestinal cancer. *J. Clin. Invest.* **130**, 5976–5988 (2020).
10. Karikó, K., Buckstein, M., Ni, H. & Weissman, D. Suppression of RNA recognition by Toll-like receptors: the impact of nucleoside modification and the evolutionary origin of RNA. *Immunity* **23**, 165–175 (2005).
11. Nelson, J. et al. Impact of mRNA chemistry and manufacturing process on innate immune activation. *Sci. Adv.* **6**, eaaz6893 (2020).
12. Vormehr, M. et al. Dexamethasone premedication suppresses vaccine-induced immune responses against cancer. *Oncoimmunology* **9**, 1758004 (2020).
13. Copeland, S. et al. Acute inflammatory response to endotoxin in mice and humans. *Clin. Diagn. Lab. Immunol.* **12**, 60–67 (2005).
14. Mitchell, W. M., Nicodemus, C. F., Carter, W. A., Horvath, J. C. & Strayer, D. R. Discordant biological and toxicological species responses to TLR3 activation. *Am. J. Pathol.* **184**, 1062–1072 (2014).
15. Mariathasan, S. et al. Cryopyrin activates the inflammasome in response to toxins and ATP. *Nature* **440**, 228–232 (2006).
16. Broz, P. & Dixit, V. M. Inflammasomes: mechanism of assembly, regulation and signalling. *Nat. Rev. Immunol.* **16**, 407–420 (2016).
17. Zhong, Z. et al. TRPM2 links oxidative stress to NLRP3 inflammasome activation. *Nat. Commun.* **4**, 1611 (2013).
18. Nalle, S. C. et al. Aquaporin-3 regulates endosome-to-cytosol transfer via lipid peroxidation for cross presentation. *Plos ONE* **15**, e0238484 (2020).
19. Dower, S. K. et al. The cell surface receptors for interleukin-1α and interleukin-1β are identical. *Nature* **324**, 266–268 (1986).
20. Gabay, C., Lamacchia, C. & Palmer, G. IL-1 pathways in inflammation and human diseases. *Nat. Rev. Rheumatol.* **6**, 232–241 (2010).
21. Li, J. et al. CD3 bispecific antibody–induced cytokine release is dispensable for cytotoxic T cell activity. *Sci. Transl. Med.* **11**, eaax8861 (2019).
22. Giavridis, T. et al. CAR T cell-induced cytokine release syndrome is mediated by macrophages and abated by IL-1 blockade. *Nat. Med.* **24**, 731–738 (2018).
23. Norelli, M. et al. Monocyte-derived IL-1 and IL-6 are differentially required for cytokine-release syndrome and neurotoxicity due to CAR T cells. *Nat. Med.* **24**, 739–748 (2018).
24. Eisenberg, S. P. et al. Primary structure and functional expression from complementary DNA of a human interleukin-1 receptor antagonist. *Nature* **343**, 341–346 (1990).
25. Hannum, C. H. et al. Interleukin-1 receptor antagonist activity of a human interleukin-1 inhibitor. *Nature* **343**, 336–340 (1990).
26. Carter, D. B. et al. Purification, cloning, expression and biological characterization of an interleukin-1 receptor antagonist protein. *Nature* **344**, 633–638 (1990).
27. Cagigi, A. & Loré, K. Immune responses induced by mRNA vaccination in mice, monkeys and humans. *Vaccines (Basel)* **9**, 61 (2021).
28. Bourke, E. et al. IL-1β scavenging by the type II IL-1 decoy receptor in human neutrophils. *J. Immunol.* **170**, 5999–6005 (2003).
29. Anandasabapathy, N. et al. Efficacy and safety of CDX-301, recombinant human Flt3L, at expanding dendritic cells and hematopoietic stem cells in healthy human volunteers. *Bone Marrow Transpl.* **50**, 924–930 (2015).
30. Eeckhout, B. V. D., Tavernier, J. & Gerlo, S. Interleukin-1 as innate mediator of T cell immunity. *Front. Immunol.* **11**, 621931 (2021).
31. Yadav, M. et al. Predicting immunogenic tumour mutations by combining mass spectrometry and exome sequencing. *Nature* **515**, 572–576 (2014).
32. Bonifant, C. L., Jackson, H. J., Brentjens, R. J. & Curran, K. J. Toxicity and management in CAR T-cell therapy. *Mol. Ther. Oncolytics* **3**, 16011 (2016).
33. Buschmann, M. D. et al. Nanomaterial delivery systems for mRNA vaccines. *Vaccines (Basel)* **9**, 65 (2021).
34. Seok, J. et al. Genomic responses in mouse models poorly mimic human inflammatory diseases. *Proc. Natl Acad. Sci. USA* **110**, 3507–3512 (2013).
35. Monteagudo, L. A., Boothby, A. & Gertner, E. Continuous intravenous anakinra infusion to calm the cytokine storm in macrophage activation syndrome. *ACR Open Rheumatol.* **2**, 276–282 (2020).
36. Huet, T. et al. Anakinra for severe forms of COVID-19: a cohort study. *Lancet Rheumatol.* **2**, e393–e400 (2020).
37. Cauchois, R. et al. Early IL-1 receptor blockade in severe inflammatory respiratory failure complicating COVID-19. *Proc. Natl Acad. Sci. USA* **117**, 18951–18953 (2020).
38. Ji, D. X. et al. Type I interferon-driven susceptibility to *Mycobacterium tuberculosis* is mediated by IL-1Ra. *Nat. Microbiol.* **4**, 2128–2135 (2019).
39. Hawash, M. B. F. et al. Primate innate immune responses to bacterial and viral pathogens reveals an evolutionary trade-off between strength and specificity. *Proc. Natl Acad. Sci. USA* **118**, e2015855118 (2021).
40. Krienke, C. et al. A noninflammatory mRNA vaccine for treatment of experimental autoimmune encephalomyelitis. *Science* **371**, 145–153 (2021).
41. Miao, L. et al. Delivery of mRNA vaccines with heterocyclic lipids increases anti-tumor efficacy by STING-mediated immune cell activation. *Nat. Biotechnol.* **37**, 1174–1185 (2019).
42. Lonez, C. et al. Cationic lipid nanocarriers activate Toll-like receptor 2 and NLRP3 inflammasome pathways. *Nanomed. Nanotechnol. Biol. Med.* **10**, 775–782 (2014).
43. Zhang, H. et al. Delivery of mRNA vaccine with a lipid-like material potentiates antitumor efficacy through Toll-like receptor 4 signaling. *Proc. Natl Acad. Sci. USA* **118**, e2005191118 (2021).
44. Ndeupen, S. et al. The mRNA-LNP platform's lipid nanoparticle component used in preclinical vaccine studies is highly inflammatory. *iScience* **24**, 103479 (2021).
45. Zanoni, I. et al. An endogenous caspase-11 ligand elicits interleukin-1 release from living dendritic cells. *Science* **352**, 1232–1236 (2016).

Methods

Mice. C57BL/6J mice (stock 000664) and *Il1rn*$^{-/-}$ mice (B6.129S-Il1rntm1Dih/J, stock 004754) were purchased from The Jackson Laboratory. *Il1r1*$^{-/-}$ mice were obtained from The Jackson Laboratory (B6.129S7-Il1r1tm1Imx/J, stock 003245) and backcrossed for eight generations to C57BL/6N mice (The Jackson Laboratory). *Nlrp3*$^{-/-}$ mice (also known as *Cias1*$^{-/-}$ mice) and *Gsdmd*$^{-/-}$ mice have been described[15,46]. Age-matched (5–15 weeks) female animals were used throughout all experiments. Mice were maintained in a specific-pathogen-free facility, in individually ventilated cages within animal rooms maintained on a 14-h/10-h, light/dark cycle. Animal rooms were temperature- and humidity-controlled, at 68–79 °F and 30–70%, respectively, with 10 to 15 room air exchanges per hour. All animal studies were reviewed and approved by Genentech's Institutional Animal Care and Use Committee.

Depletion, inhibition and blocking experiments. Buffy coats or whole blood were obtained from voluntary, healthy human donors participating in the Genentech blood donor program, after written, informed consent from the Western Institutional Review board. As anonymous donors were used, covariate-relevant participant characteristics such as age and sex were not available. PBMCs were isolated by density centrifugation using SepMate-50 tubes and Lymphoprep Medium (both from StemCell Technologies). Red blood cells were lysed with ACK lysis buffer (Gibco) and remaining blood cells were passed twice through a 70-µm filter. Monocytes or neutrophils were depleted from either PBMCs or whole blood with anti-human CD14 MicroBeads (130-050-201, Miltenyi Biotec), EasySep Human CD14 Positive Selection Kit II (17858, StemCell Technologies) or EasySep HLA Chimerism Whole Blood CD66b Positive Selection Kit (17882, StemCell Technologies), respectively. NHP PBMCs were ordered frozen (from iQ Biosciences), thawed and rested overnight before RNA-LPX treatment.

First, 1.5–3.5 × 10^5 cells were plated on 96-U-well plates and stimulated with 1 µg ml^{-1} LPS-EK (InvivoGen), 10 µg ml^{-1} Nigericin (InvivoGen) or RNA-LPX with or without 0.1–5 µM MCC950 (Sigma), 1–50 µM Necrosulfonamide (Sigma-Aldrich), 1–30 µM zVAD-FMK (Promega), 0.5 µg ml^{-1} R848 (InvivoGen), 1–50 µM DPI (Calbiochem), 1–50 µM BAPTA-AM (Sigma-Aldrich), 1–100 µg ml^{-1} anti-IL-1β neutralizing antibodies (InvivoGen) or 1–100 µg ml^{-1} control IgG1 antibodies (InvivoGen). Of note, as R848, LPS or RNA-LPX were not washed away between priming (signal 1) and triggering (signal 2) to account for possible activation of alternative NLRP3 inflammasome[47]. After 17 h, the cells were pelleted down, and the supernatants were collected and stored at −80 °C until analysis.

RNA-LPX, modRNA-LNP, TLR agonists and immune challenge. RNAs were synthesized by Genentech. RNAs encoding for either MC38-derived neoantigens or eGFP have been described[1,12]. RNA was formulated with liposomes consisting of DOTMA and DOPE at a charge ratio (+):(−) of 1.3:2, yielding negatively charged RNA-LPX[1]. For some in vitro experiments using RNA-LPX, RNA was synthesized using pseudouridine instead of uridine and 5-methyl-cytosine instead of cytosine to reduce TLR activation[10].

For in vitro experiments using modRNA-LNP, RNA was synthesized using 1-methyl-pseudouridine instead of uridine[3], capping was performed cotranscriptionally using a trinucleotide cap 1 analog (CleanCap AG (3′ OMe) m7(3′OMeG)(5′)ppp(5′)(2′OMeA)pG, Trilink)[3] and RNA was purified with cellulose treatment[48]. Finally, modRNA-LNP was formulated with a lipid mixture consisting of an ionizable lipid (either Dlin-MC3-DMA or SM-102), distearoylphosphatidylcholine (DSPC), cholesterol and PEG-lipid (at molar ratios of 50:20:28:2 for the MC3 formulation or 50:10:38.5:1.5 for the SM-102 formulation) using a microfluidic mixer, as previously described[49].

For in vivo experiments, RNA-LPX (dose indicated in respective figure legends), 10 µg of ODN1826 VacciGrade (InvivoGen), 1 µg of LPS-EB VacciGrade (InvivoGen) or 1 × 10^8 HKLM (InvivoGen) was injected intravenously or 300 µg of DMXAA (InvivoGen), 30 µg of mFlt3L (Genentech), 500 µg of rat IgG2a isotype (BioXCell) or 500 µg of anti-Ly6G antibodies (BioXCell) was injected intraperitoneally into C57BL/6 mice as described in the respective figures. At 4–6 h after immune challenge, mice were bled for cytokine analysis. Rectal body temperature and body weight were measured for a total of 6 d following exposure or until the values reached pretreatment levels.

TDB experiments in tumor-bearing mice. Generation and verification of ID8/LyPD1 cells has been described[50]. Briefly, ID8/LyPD1 is a murine ID8 ovarian cancer cell line expressing the tumor-associated antigen LY6/PLAUR Domain-containing 1 gene (LyPD1), which was generated by lentiviral transduction. Cells were passaged twice in vivo for faster growth kinetics before generating master and working cell banks, of which third and fourth passages were used for tumor experiments. Then, 4 × 10^6 ID8/LyPD1 tumor cells in Hank's Balanced Salt Solution and Matrigel were inoculated subcutaneously in the 2/3 mammary fat pad of wildtype and *Il1rn*$^{-/-}$ mice. Tumor sizes were measured unblinded with a caliper twice a week and tumor volumes were calculated by using the equation ($a^2 \times b$)/2 (a, width; b, length). T cell retargeting to LyPD1 was achieved by administration of mouse CD3-bispecific TDB antibodies[21,50]. Once tumors reached the target volume of 100–300 mm^3 (median 150 mm^3, approximately 3–4 weeks after implantation), animals were randomly divided into treatment groups and injected intravenously with 10 mg kg^{-1} anti-LyPD1/anti-CD3 TDB antibodies (diluted in 20 mM histidine acetate pH 5.5, 240 mM sucrose, 0.02% Tween-20) or vehicle only. Animals were euthanized 24 h after TDB administration for flow cytometric analysis or when exhibiting signs of impaired health.

Blood and tissue preparation. Cardiac puncture under deep terminal anesthesia was used to collect a large volume of whole blood for downstream in vitro assays. Whole blood was stored in EDTA polypropylene tubes (Sarstedt) and red blood cells were lysed with ACK lysis buffer (Gibco). Retro-orbital bleeding under isoflurane anesthesia was used to collect peripheral blood samples. Blood was stored in gel-separator polypropylene tubes (Sarstedt) and incubated for 15 min at room temperature, after which the coagulated blood samples were centrifugated at 2,300*g* for 5 min. Clear serum was transferred to new tubes and stored at −80 °C for downstream assays.

Spleens were collected in cold PBS and single-cell suspensions were generated by mashing the spleen tissue through a 70-µm cell strainer (BD Falcon) in Hank's-based Cell Dissociation Buffer (Gibco) supplemented with Liberase (Roche) and DNase I (ThermoFisher). Red blood cells were lysed with ACK lysis buffer (Gibco).

Flow cytometry. Single-cell suspensions were incubated in FACS buffer (PBS supplemented with 0.5% BSA and 0.05% sodium azide) containing anti-mouse CD16/CD32 (Mouse Fc Block, BD) or Human TruStain FcX (Human Fc Block, Biolegend) for 10 min before and during staining with the indicated antibodies. Staining reagents for murine cells included FITC anti-CD169 (3D6.112, Biolegend), PE anti-IL-1α (ALF-161, eBioscience), PerCP-Cy5.5 anti-CD3 (17A2, Biolegend), BUV395 anti-B220 (RA3-6B2, BD), PE anti-NK1.1 (PK136, Biolegend), BV510 anti-CD11c (N418, Biolegend), BUV737 anti-CD4 (GK1.5, BD), VioBlue anti-CD11b (M1/70.15.11.5, Miltenyi Biotec), APC anti-CD115 (AFS98, Biolegend), FITC anti-CD11b (M1/70, Biolegend), PeCy7 anti-pro-IL-1β (NJTEN3, eBioscience), BV711 anti-F4/80 (BM8, Biolegend), AF700 anti-Ly-6C (HK1.4, Biolegend), AF647 anti-Siglec-F (E50-2440, BD), BV785 anti-Ly-6G (1A8, Biolegend), APC anti-CD209b (22D1, eBioscience), FITC PD-1 (29F.1A12, Biolegend), AF700 CD8 (KT15, BioRad), V500 CD90.1 (53-2.1 Biolegend), APC-Cy CD4 (GK1.5, BD Biosciences), APC-H7 CD19 (1D3, BD Biosciences), BUV395 KLRG1 (2F1, BD Biosciences), PerCP-eFluor710 CD127 (SB/199, Invitrogen), PE TCF1/TCF7 (C63D9, Cell Signaling Technology), AF488 IFNg (XMG1.2, Biolegend), BUV395 TCRb (H57-597, BD Biosciences), PeCy7 CD8 (53-6.7, BD Biosciences), BV510 B220 (RA3-6B2, Biolegend), BV421 TNF (MP6-XT22, Biolegend), BV785 CD4 (RM4-5, Biolegend), APC CD107a (1D4B, Biolegend), PE IL-1R1 (JAMA-147, Biolegend) and BV421 IL-1R2 (4E2, BD Biosciences). Intracellular Fixation & Permeabilization Buffer Set (88-8824-00, eBioscience) was used for intracellular staining of cytokines. Foxp3/Transcription Factor Staining Buffer Set (00-5523-00, eBioscience) was used for intranuclear staining of TCF1. Mitochondrial ROS levels in human monocytes were measured using MitoSOX Red Mitochondrial Superoxide Indicator (Invitrogen). To assess purity of CD14- or CD66b-depleted human cell populations, PerCP-Vio700 anti-CD14 (TÜK4, Miltenyi Biotec), PE anti-CD66b (G10F5, Biolegend), PeCy7 anti-CD3 (SK7, BD), APC-H7 anti-CD19 (SJ25C1 BD) and V500 anti-HLA-DR (G46-6, BD) were used. To study human and NHP monocyte frequencies, cross-species reactive APC anti-CD14 (M5E2, Biolegend) was used. Cells were stained on ice for extracellular markers for 20–30 min followed by staining for intracellular markers for 60 min, and filtered using 30–40-µm filter plates (PALL). Samples were acquired with BD FACSDiva software v.8.0 on a BD FACSymphony (BD) and analyzed with Flow Jo v.10.7.1 (TreeStar). Dead cells and cell aggregates were excluded from analyses by Fixable Viability Dye eFluor 780 (eBioscience), LIVE/DEAD Fixable Near-IR (Dead Cell Stain Kit for 633- or 635-nm excitation, Invitrogen) or LIVE/DEAD Fixable Blue (Dead Cell Stain Kit for UV excitation, Invitrogen) staining and forward scatter area (FSC-A)/forward scatter height (FSC-H) characteristics.

Murine bone-marrow-derived cultures. Bone marrow cells collected from wildtype or *Il1r1*$^{-/-}$ mice were differentiated in RPMI with 10% heat-inactivated fetal bovine serum (Gibco), 1% Glutamax (Gibco), 2-mercaptoethanol (55 µM, Gibco), 100 ng ml^{-1} recombinant mFlt3L (Peprotech) and 10 ng ml^{-1} mGMCSF (Peprotech) for 13 d. Differentiated, immature cells were then plated at 300,000 cells per well on a 96-U-well plate and stimulated for 16 h with 5 µg ml^{-1} RNA-LPX (Genentech) or 0.1 µg ml^{-1} Pam3CSK4, 0.1 µg ml^{-1} FSL1, 10^8 bacteria per ml HKLM, 10 µg ml^{-1} poly I:C, 0.05 µg ml^{-1} LPS-EK, 0.1 µg ml^{-1} FLA-ST, 0.1 µg ml^{-1} ssRNA40/Lyovec, 0.1 µg ml^{-1} CL097, 0.1 µg ml^{-1} R848, 0.1 µg ml^{-1} R837, 5 µM ODN1585, 5 µM ODN1826, 5 µM ODN2395, 10 µg ml^{-1} c-di-AMP, 10 µg ml^{-1} DMXAA or 10 µg ml^{-1} 2′3′-c-di-AM(PS)2 (Rp,Rp) (all from InvivoGen). After stimulation, the cells were pelleted down, and the supernatants were collected and stored at −80 °C until analysis.

Luminex/ELISA assays. Serum concentrations of murine cytokines were determined using a bead-based, Cytokine & Chemokine Convenience 26-Plex Mouse ProcartaPlex multiplex immunoassay supplemented with murine

IFNα ProcartaPlex (ThermoFisher Scientific) according to the manufacturer's instructions. Serum concentrations of soluble receptors were determined using MILLIPLEX MAP Mouse Soluble Cytokine Receptor Magnetic Bead Panel (Millipore). Acute phase proteins were determined using MILLIPLEX MAP Mouse Acute Phase Magnetic Bead Panel 2 (Millipore). ELISA was used for the detection of mIL-1α (R&D Systems), mIL-1ra (Abcam) and mSAA3 (Sigma-Aldrich).

For the detection of human cytokines in vitro, MILLIPLEX MAP Human Cytokine/Chemokine Magnetic Bead Panel Premixed 30-plex assay (Millipore) was used according to the manufacturer's instructions. For the detection of human cytokines in vivo, Simoa assay (Quanterix) and DiscoveryMAP Multiplexes (Myriad RBM) were used according to the manufacturer's instructions. For the detection of NHP cytokines in vitro, MILLIPLEX MAP Non-Human Primate Cytokine Magnetic Bead Panel Premixed 23-plex assay (Millipore) was used according to the manufacturer's instructions. Values below the lower limit of quantification were set to zero. Luminex data were collected on Flex-Map 3D v.3.2 (Luminex Corporation) and analyzed with Bio-Plex Manager 6.1.1 and Microsoft Excel v.16.16.27.

Clinical trial design and samples. A first-in-human phase 1b study of RO7198457 (Autogene cevumeran), a systemically administered RNA-LPX, in combination with the anti-PD-L1 antibody atezolizumab was conducted in patients with locally advanced or metastatic solid tumors[4,5] (ClinicalTrials.gov identifier NCT03289962). Briefly, RO7198457 was GMP-manufactured on a per-patient basis and contained up to 20 tumor-specific neoepitopes. The study protocols were approved by the relevant authorities and ethics committee. The study was conducted in accordance with all applicable laws and regulations, and in agreement with the International Council on Harmonisation of Good Clinical Practice (ICH-GCP) guidelines and the Declaration of Helsinki. Written, informed consent was obtained from all patients before enrollment. RO7198457 was administered intravenously at a dose of 25 µg and atezolizumab at a dose of 1,200 mg. Blood samples were obtained before vaccination (predose), and at 4–6 h and 24 h after RO7198457 administration. Plasma cytokines were measured from nine patients as shown in Figs. 1i and 3d (sample selection was based on plasma availability and existing ELISPOT data, while excluding patients that had received steroids at the time of vaccination).

Statistical analyses and data presentation. Statistical analyses and graphing were performed using GraphPad Prism v.9.1.0 for Mac OS. Illustrations were created with BioRender.com. All results are expressed as mean ± s.e.m. or median without interquartile range as indicated. Unpaired two-tailed Student's *t*-test was used for comparison of two groups. One-way analysis of variance (ANOVA) was performed when more than two groups were compared, and multiple comparisons were corrected using Dunnett's post hoc test or Sidak's post hoc test. Two-way ANOVA was performed when both time and genotype or treatment were compared, and multiple comparisons were corrected using Dunnett's post hoc test or Sidak's post hoc test. $^{*}P \leq 0.05$, $^{**}P \leq 0.01$, $^{***}P \leq 0.001$ and $^{****}P \leq 0.0001$. No statistical methods were used to predetermine sample size for animal experiments.

Reporting Summary. Further information on research design is available in the Nature Research Reporting Summary linked to this article.

Data availability

The data that support the findings of this study are available from the corresponding author upon reasonable request.

Code availability

No custom code or specific mathematical algorithms were used in this study.

References

46. Kayagaki, N. et al. Caspase-11 cleaves gasdermin D for non-canonical inflammasome signalling. *Nature* **526**, 666–671 (2015).
47. Gaidt, M. M. & Hornung, V. Alternative inflammasome activation enables IL-1β release from living cells. *Curr. Opin. Immunol.* **44**, 7–13 (2017).
48. Baiersdörfer, M. et al. A facile method for the removal of dsRNA contaminant from in vitro-transcribed mRNA. *Mol. Ther. Nucleic Acids* **15**, 26–35 (2019).
49. Sabnis, S. et al. A novel amino lipid series for mRNA delivery: improved endosomal escape and sustained pharmacology and safety in non-human primates. *Mol. Ther.* **26**, 1509–1519 (2018).
50. Lo, A. A. et al. Anti-LYPD1/CD3 T-cell-dependent bispecific antibody for the treatment of ovarian cancer. *Mol. Cancer Ther.* **20**, 1–10 (2021).

Acknowledgements

We thank N. Kayagaki, S. Schock, B. Lee, T. Junttila, I. Balter, K. Nutsch, A.-H. Herzner, J. Hagar, S. Cullen, R. Barreira da Silva, C. Carbone, A. Ritter, K. Banta, A. Chitre Elgin, A. Castiglioni, V. Romeo, V. Leveque, R. Sabado, B. Lauffer, V. Sunkari and the FACS laboratory and the Luminex core for technical advice and support; C. Cox, K. Newton, G. Strasser, B. Grellman, D. Montoya, T. Scholl and S. Powell for assistance with breeding and acquisition of animals; I. Rhee for comments; and the GO39733 study team for support in accessing and interpreting clinical data.

Author contributions

S.T., A.-J.T., P.H., J.O., L.D. and I.M. designed, planned and/or supervised the study. S.T., A.-J.T., P.H., J.O., A.P.-M., Y.O. and M.J.M. performed experiments under the supervision of J.M.S., W.Y., C.C.d.l.C., U.S., L.D. and I.M. L.K. and M.Y. analyzed clinical human samples. S.W., E.C.F. and Z.A.A. prepared vaccine components under the supervision of B.H. and C.B. S.T., A.-J.T., P.H., J.O., M.J.M., J.M.S., W.Y., C.C.d.l.C., B.H., C.B., U.S., L.D. and I.M. contributed to interpretation of the data. S.T. wrote the paper with edits from I.M. and input from co-authors.

Competing interests

All authors except U.S. are current or former employees of Genentech (South San Francisco, USA). U.S. is a management board member and an employee at BioNTech AG (Mainz, Germany), and inventor on patents and patent applications related to RNA vaccines used in this study. U.S. has securities from BioNTech AG.

Additional information

Extended data is available for this paper at https://doi.org/10.1038/s41590-022-01160-y.

Supplementary information The online version contains supplementary material available at https://doi.org/10.1038/s41590-022-01160-y.

Correspondence and requests for materials should be addressed to Ira Mellman.

Peer review information *Nature Immunology* thanks the anonymous reviewers for their contribution to the peer review of this work. Zoltan Fehervari was the primary editor on this article and managed its editorial process and peer review in collaboration with the rest of the editorial team.

Reprints and permissions information is available at www.nature.com/reprints.

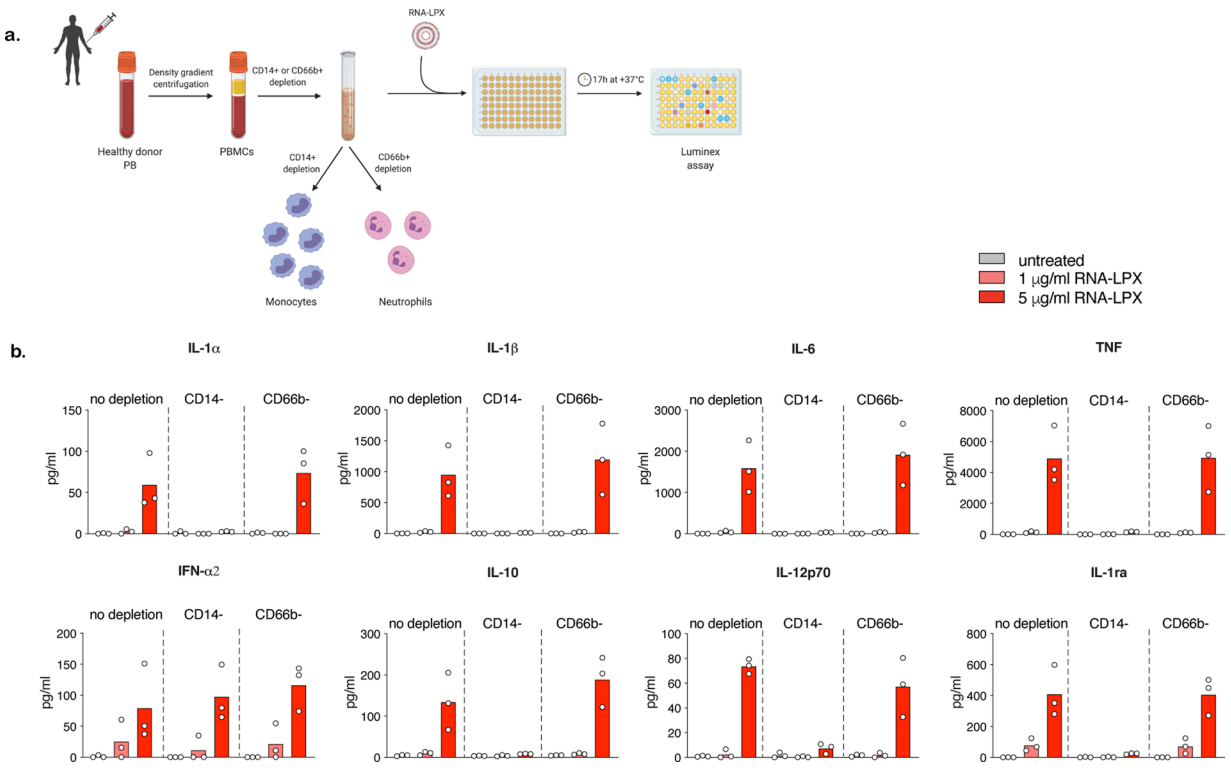

Extended Data Fig. 1 | RNA-LPX-induced cytokine response is driven by monocytes, not neutrophils. a, **b**, RNA-LPX-induced cytokines secreted by human PBMCs (n = 3) following depletion of CD14 + monocytes or CD66b + neutrophils *in vitro*. The data are representative of two independent experiments with biologically independent samples. Data presented as median.

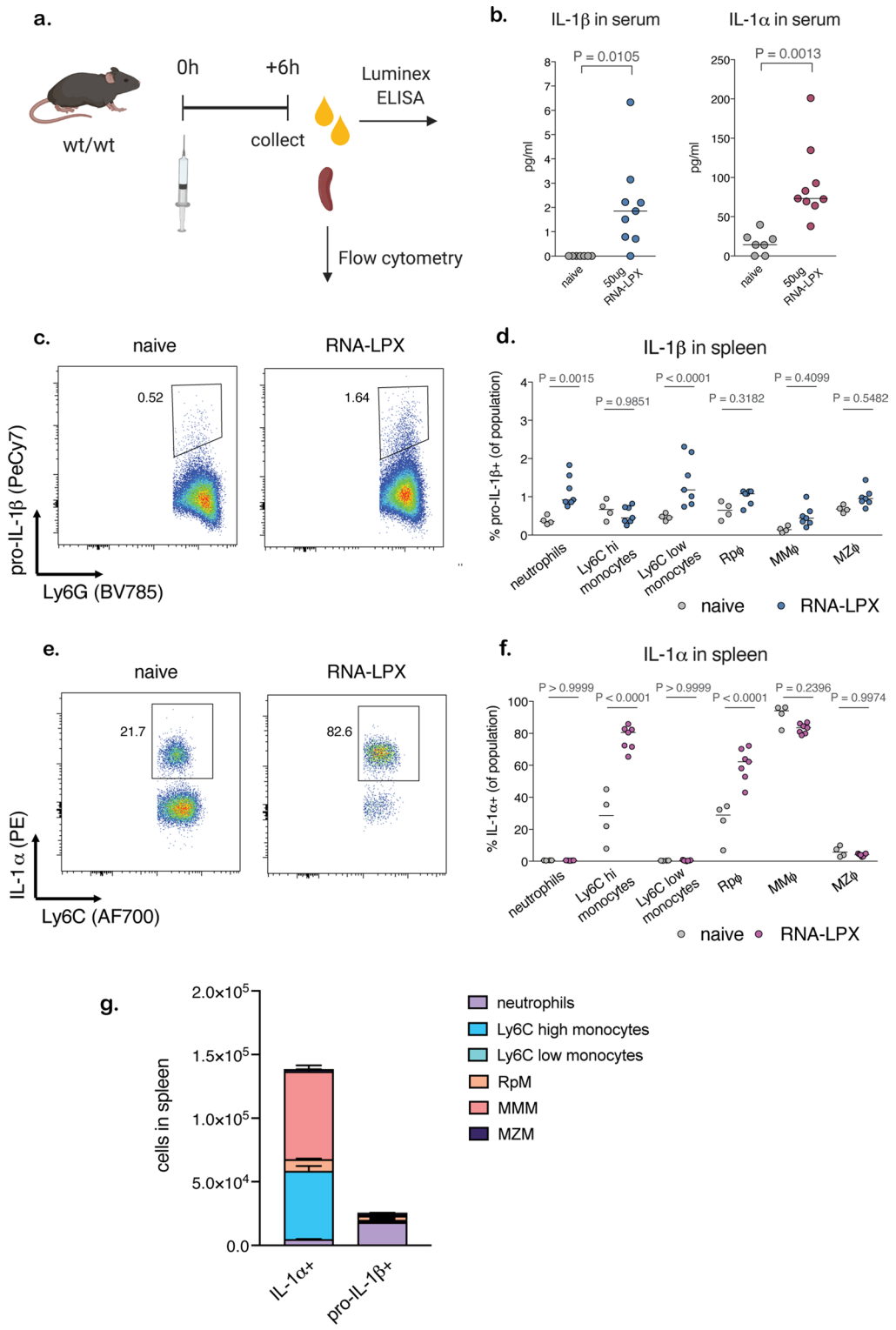

Extended Data Fig. 2 | Intravenous administration of RNA-LPX induces secretion of both IL-1β and IL-1α in C57BL/6 mice. a-g, IL-1β and IL-1α measured 6 hours after IV injection of RNA-LPX in serum (**b**, n = 9) and in splenic myeloid cell subsets (n = 7) (**c, d, e, f, g**). The data are pooled from two independent experiments with biologically independent samples (**b-f**). Significance was determined by using unpaired two-tailed Student's *t*-test (**b**) or one-way ANOVA and Tukey's multiple comparisons test (**d, f**). Data presented as mean ± SEM (**g**), otherwise median. Rpϕ, red pulp macrophage; MMϕ, marginal metallophilic macrophage; MZϕ, marginal zone macrophage.

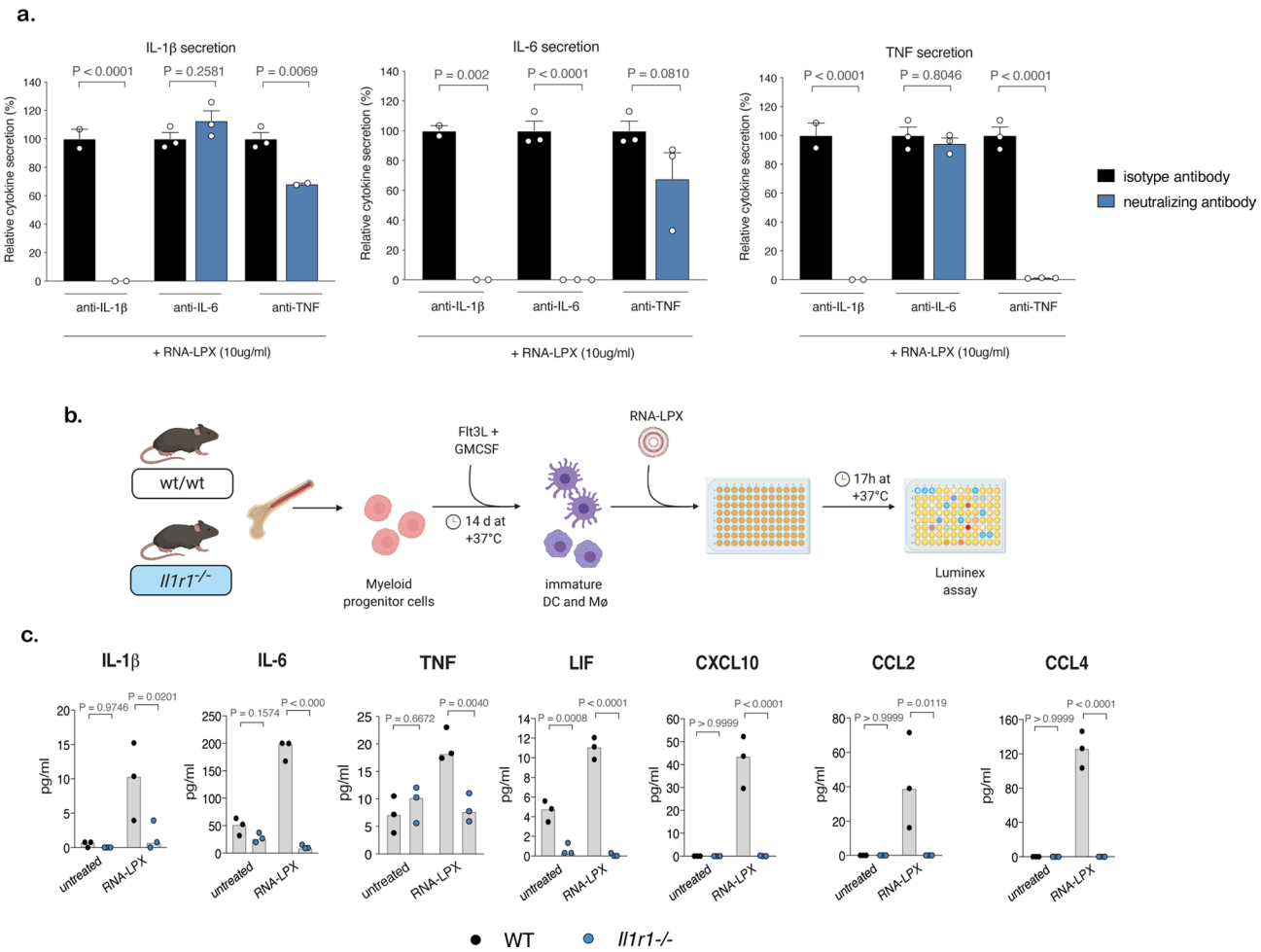

Extended Data Fig. 3 | IL-1β is released upstream of IL-6 and TNF in human PBMCs and in murine BMDCs. a, Secretion of IL-1β, IL-6 and TNF from human PBCMs (n = 3) following treatment with RNA-LPX and either isotype antibodies or neutralizing antibodies against IL-1β, IL-6 or TNF. **b, c**, Secretion of cytokines from DC/macrophage cultures derived from bone-marrow of wildtype or IL-1R1 knockout mice (n = 3) following treatment with RNA-LPX *in vitro*. The data are representative of two independent experiments with biologically independent samples. Significance was determined using one-way ANOVA and Sidak's multiple comparisons test. Data presented as mean ± SEM (**a**) or median (**c**).

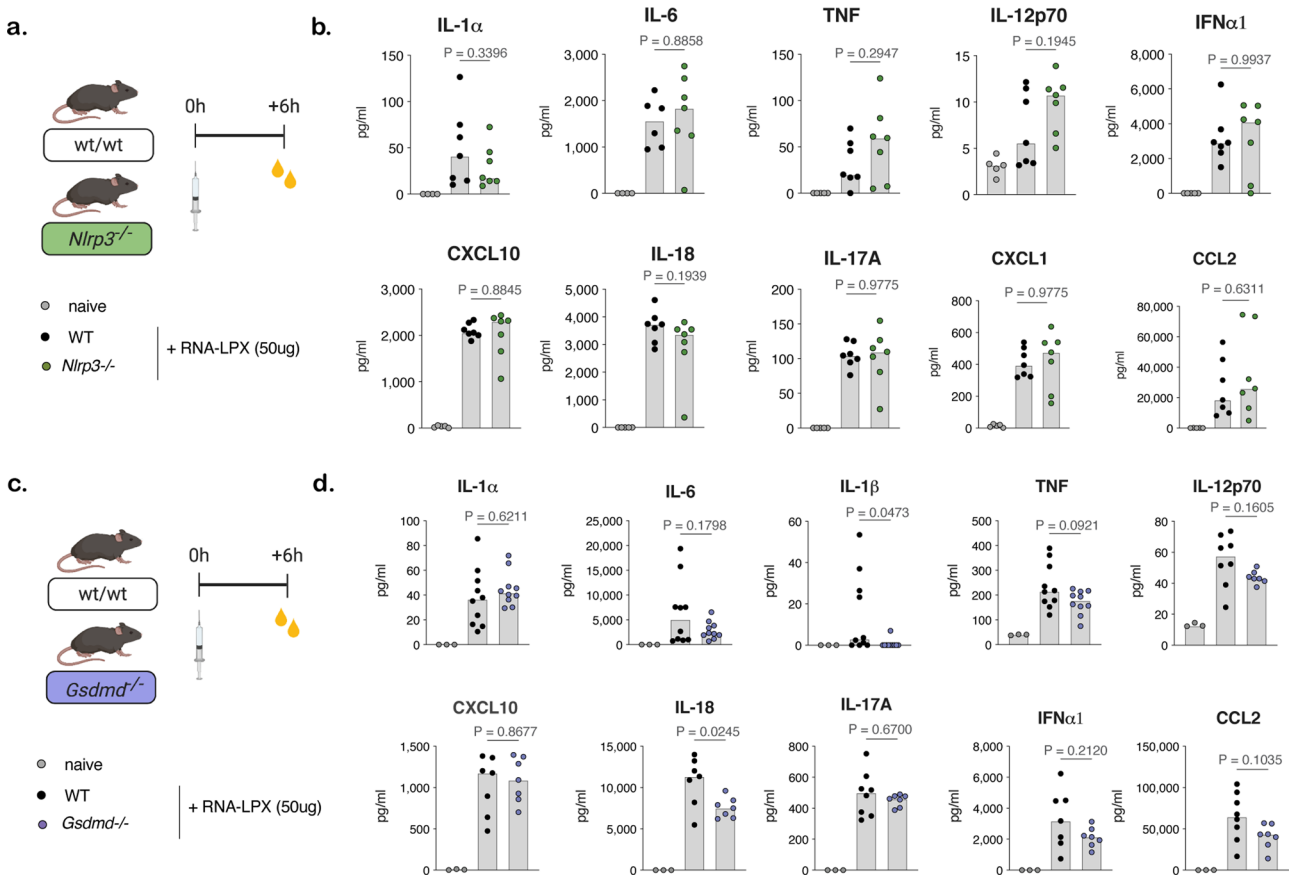

Extended Data Fig. 4 | Loss of NLRP3 inflammasome or gasdermin D does not affect RNA-LPX-induced cytokine release in C57BL/6 mice. **a**, **b**, Serum cytokine levels in wildtype and NLRP3 deficient (*Nlrp3*$^{-/-}$) mice (n = 7) after IV injection of RNA-LPX. **c, d**, Serum cytokine levels in wildtype and gasdermin D deficient (*Gsdmd*$^{-/-}$) mice (n = 7) after IV injection of RNA-LPX The data are representative of two independent experiments with biologically independent samples. Significance was determined by using one-way ANOVA and Dunnett's multiple comparisons test (**b, d**). Data presented as median.

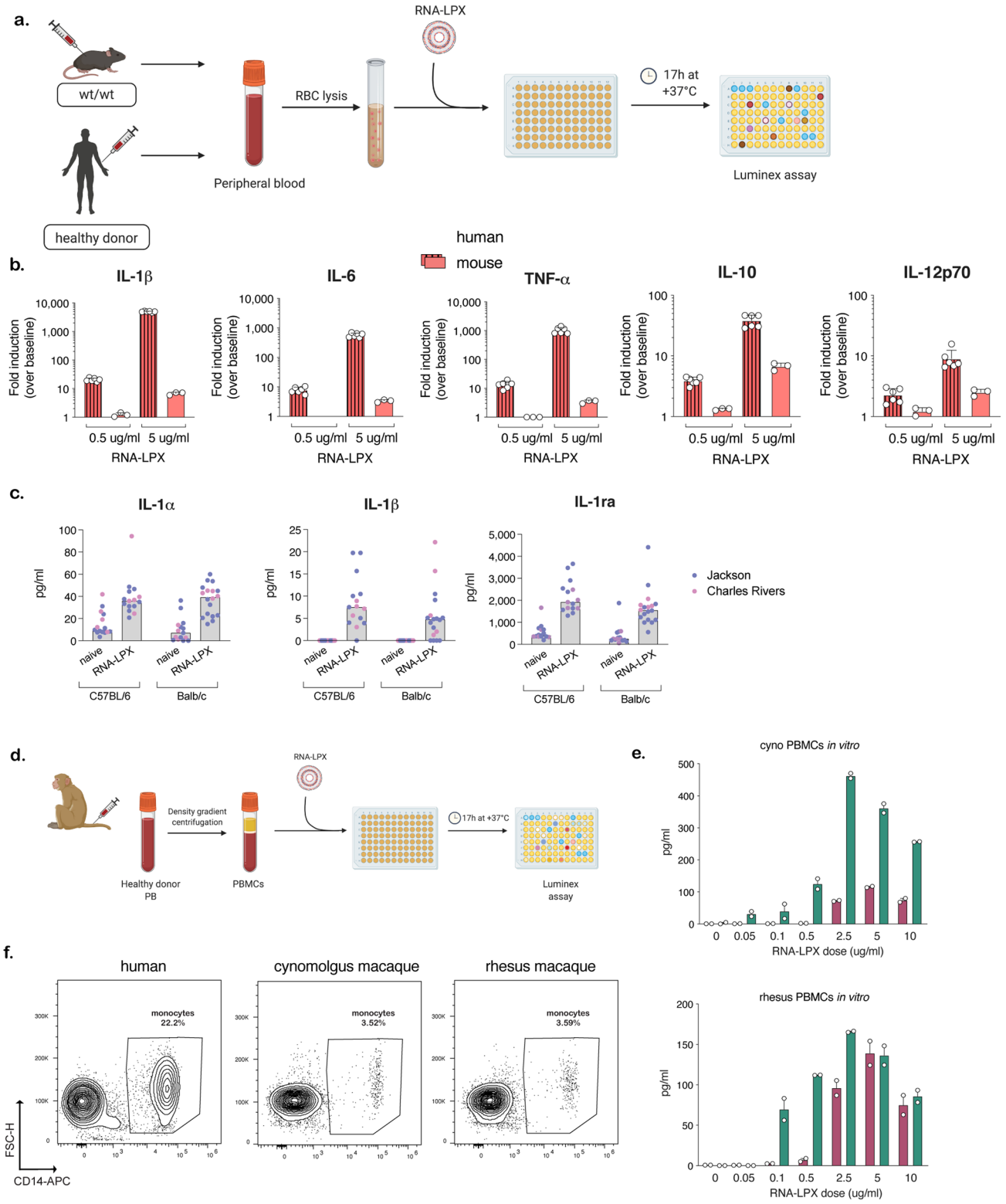

Extended Data Fig. 5 | Species-specific differences in IL-1 induction hierarchy. a, b, Fold induction of RNA-LPX-induced cytokines over baseline levels in red blood cell depleted peripheral blood cells derived either from healthy human donors (n = 6) or from naive mice (n = 3 pooled samples). **c**, Levels of serum IL-1α, IL-1β and IL-1ra 6 hr post-RNA-LPX in C57BL/6 mice (n = 15) and Balb/c mice (n = 18) ordered from different vendors. **d**, RNA-LPX-induced cytokine secretion assay using non-human primate (NHP) PBMCs. **e**, Secretion of IL-1β and IL-1ra from NHP PBMCs following treatment with RNA-LPX. **f**, Frequency of CD14 + monocytes in representative samples of human, cynomolgus macaque and rhesus macaque PBMCs. The data are representative of two independent experiments (**b, e, f**) or pooled data from three independent experiments (**c**) with biologically independent samples. Data presented as median (**c**), otherwise mean ± SEM.

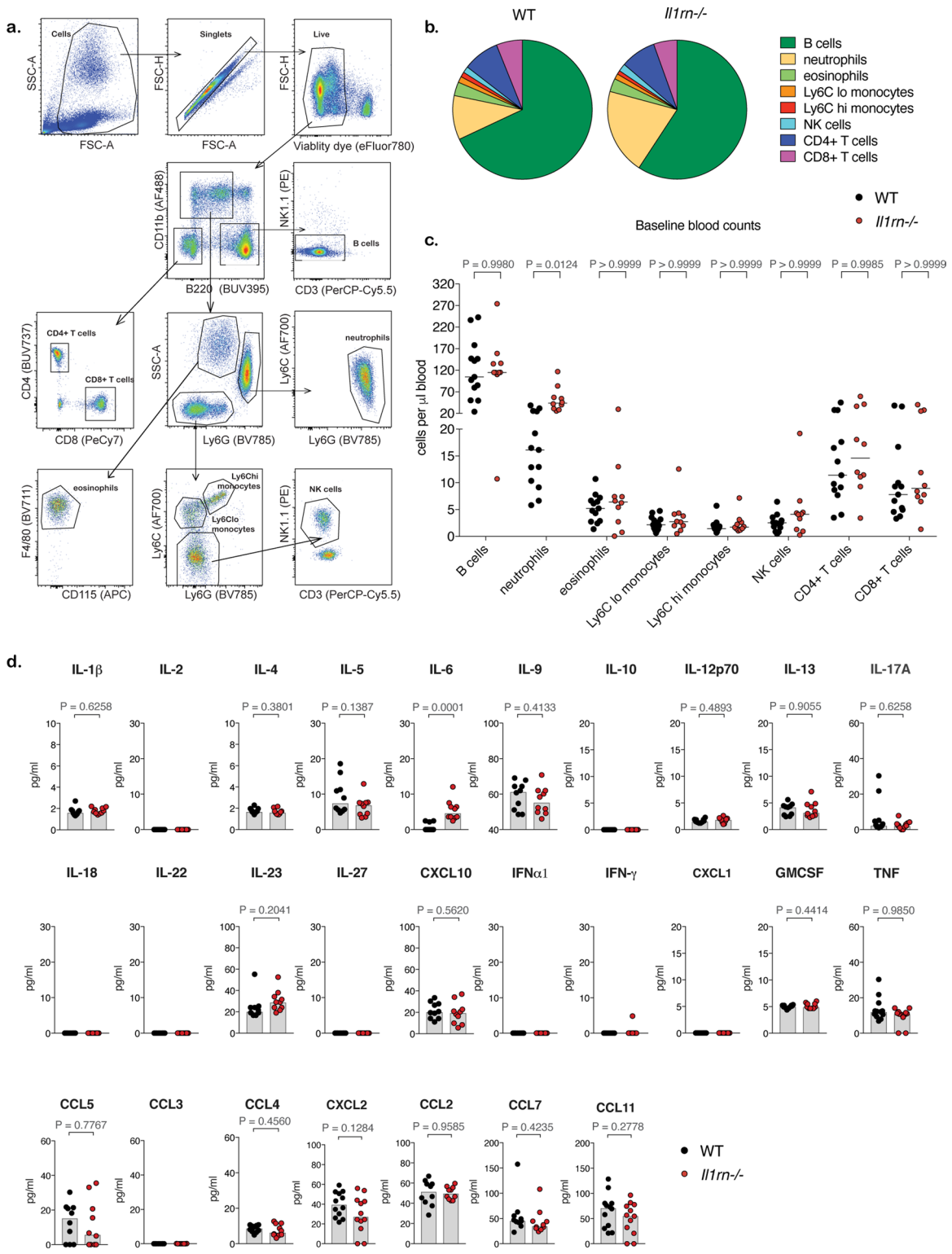

Extended Data Fig. 6 | Baseline blood in wildtype and *Il1rn*$^{-/-}$ mice. a, **b**, **c**, Blood cell composition (**a, b**), cell counts (**c**) and serum cytokines (**d**) in naïve wildtype (n = 10) and *Il1rn*$^{-/-}$ mice (n = 10). The data are pooled from two independent experiments with biologically independent samples. Significance was determined using one-way ANOVA and Sidak's multiple comparisons test (**c**) or unpaired two-tailed Student's *t*-test (**d**). Data presented as median.

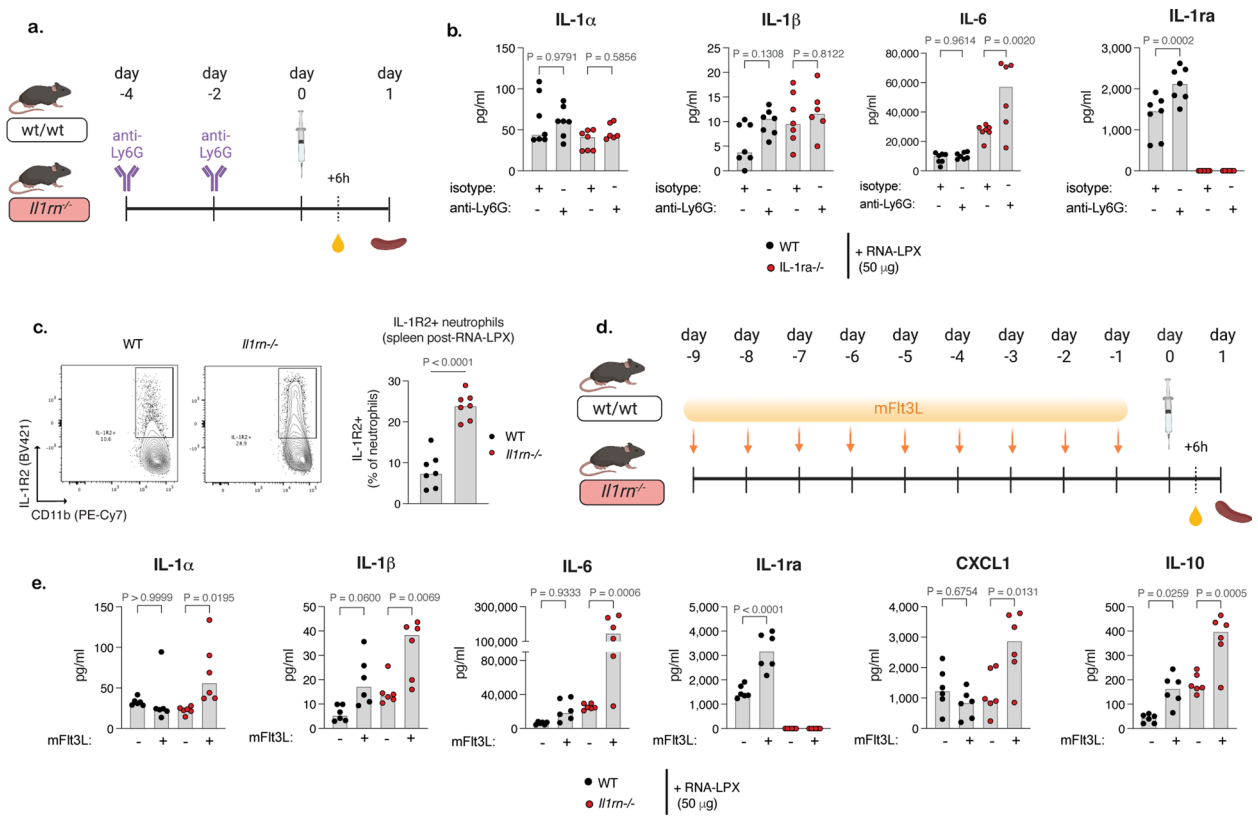

Extended Data Fig. 7 | Impact of myeloid cells on RNA-LPX induced systemic cytokine responses *in vivo*. **a**, **b**, Systemic cytokine response in Ly6G-depleted wildtype (n = 8) and *Il1rn*$^{-/-}$ mice (n = 7) following RNA-LPX administration *in vivo*. **e**, Expression of decoy receptor IL-1R2 on splenic neutrophils 24 hr post-RNA-LPX (n = 7). **f, g**, Systemic cytokine response in Flt3L-pretreated wildtype (n = 6) and *Il1rn*$^{-/-}$ mice (n = 6) following RNA-LPX administration *in vivo*. The data are representative of two independent experiments with biologically independent samples. Significance was determined by using one-way ANOVA and Tukey's multiple comparisons test (**b, e**) or by unpaired two-tailed Student's *t*-test (**c**). Data presented as median.

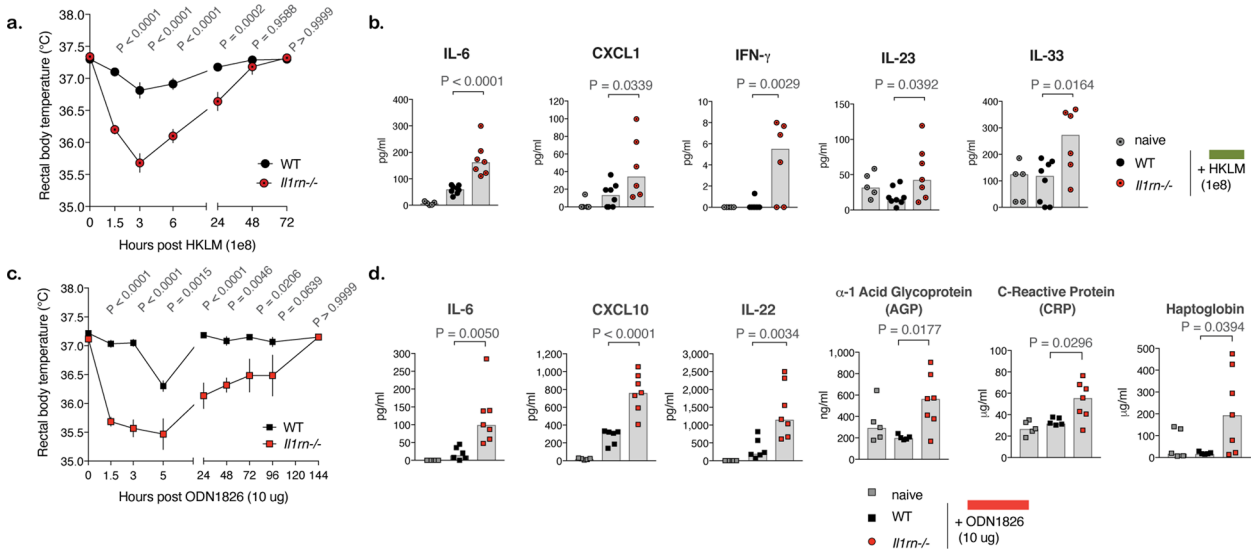

Extended Data Fig. 8 | IL-1ra downregulates the response to different TLR stimuli *in vivo*. Core body temperature (**a, c**) and serum proteins (**b, d**) in wildtype (n = 7) and *Il1rn*$^{-/-}$ mice (n = 7) after systemic administration of HKLM or ODN1826. Significance was determined using two-way repeated measures ANOVA and Sidak's multiple comparisons test (**a, c**) or one-way ANOVA and Dunnett's multiple comparisons test (**b, d**). Data presented as median (**b, d**), otherwise mean ± SEM.

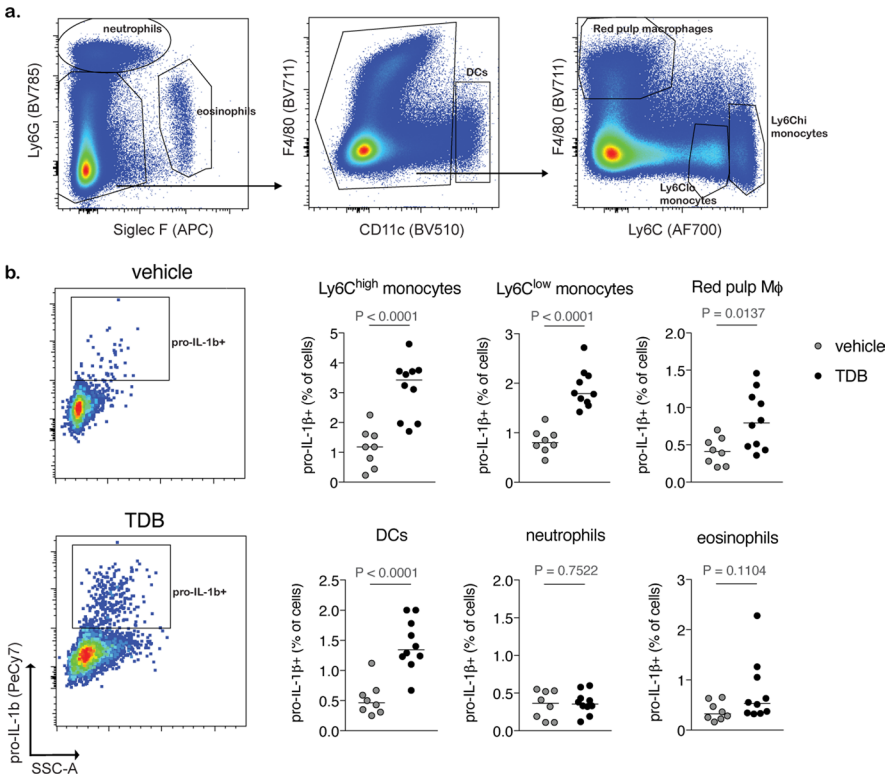

Extended Data Fig. 9 | TDB administration induces IL-1β expression in splenic myeloid cells *in vivo*. a, **b**, Gating strategy (**a**) and expression of pro-IL-1β (**b**) in spleen cell subsets following vehicle (n = 8) or TDB administration (n = 10) in ID8/LyPD1 tumor-bearing mice. The data are pooled from two independent experiments with biologically independent samples. Significance was determined using unpaired two-tailed Student's *t*-test. Horizontal bars indicate median.

nature research

Corresponding author(s): Ira Mellman

Last updated by author(s): 02/09/2022

Reporting Summary

Nature Research wishes to improve the reproducibility of the work that we publish. This form provides structure for consistency and transparency in reporting. For further information on Nature Research policies, see our Editorial Policies and the Editorial Policy Checklist.

Statistics

For all statistical analyses, confirm that the following items are present in the figure legend, table legend, main text, or Methods section.

n/a	Confirmed
☐	☒ The exact sample size (*n*) for each experimental group/condition, given as a discrete number and unit of measurement
☐	☒ A statement on whether measurements were taken from distinct samples or whether the same sample was measured repeatedly
☐	☒ The statistical test(s) used AND whether they are one- or two-sided *Only common tests should be described solely by name; describe more complex techniques in the Methods section.*
☒	☐ A description of all covariates tested
☐	☒ A description of any assumptions or corrections, such as tests of normality and adjustment for multiple comparisons
☐	☒ A full description of the statistical parameters including central tendency (e.g. means) or other basic estimates (e.g. regression coefficient) AND variation (e.g. standard deviation) or associated estimates of uncertainty (e.g. confidence intervals)
☐	☒ For null hypothesis testing, the test statistic (e.g. *F*, *t*, *r*) with confidence intervals, effect sizes, degrees of freedom and *P* value noted *Give P values as exact values whenever suitable.*
☒	☐ For Bayesian analysis, information on the choice of priors and Markov chain Monte Carlo settings
☒	☐ For hierarchical and complex designs, identification of the appropriate level for tests and full reporting of outcomes
☒	☐ Estimates of effect sizes (e.g. Cohen's *d*, Pearson's *r*), indicating how they were calculated

Our web collection on statistics for biologists contains articles on many of the points above.

Software and code

Policy information about availability of computer code

Data collection	Flow cytometry data were acquired with BD FACSDiva software v8.0 on a BD FACSymphony. Luminex data were collected on Flex-Map 3D version 3.2. (Luminex Corporation). No custom software codes have been developed.
Data analysis	Flow cytometry data were analyzed with Flow Jo version 10.7.1. Data was analyzed with Microsoft Excel version 16.16.27. Graphs and statistics were generated with Prism version 9.1.0. Luminex data were analyzed with Bio-Plex Manager 6.1.1.

For manuscripts utilizing custom algorithms or software that are central to the research but not yet described in published literature, software must be made available to editors and reviewers. We strongly encourage code deposition in a community repository (e.g. GitHub). See the Nature Research guidelines for submitting code & software for further information.

Data

Policy information about availability of data

All manuscripts must include a data availability statement. This statement should provide the following information, where applicable:

- Accession codes, unique identifiers, or web links for publicly available datasets
- A list of figures that have associated raw data
- A description of any restrictions on data availability

The raw data underlying the figures available to readers as source data files.

Field-specific reporting

Please select the one below that is the best fit for your research. If you are not sure, read the appropriate sections before making your selection.

☒ Life sciences ☐ Behavioural & social sciences ☐ Ecological, evolutionary & environmental sciences

For a reference copy of the document with all sections, see nature.com/documents/nr-reporting-summary-flat.pdf

Life sciences study design

All studies must disclose on these points even when the disclosure is negative.

Sample size	No sample size calculations were performed. For in vitro studies, cells or tissues from at least 3 animals per genotype or from at least 3 human donors were analyzed to ensure differences were reproducible. Larger numbers (n=7-10 per treatment group) were used in the in vivo studies using RNA-LPX, PRR agonists or TDBs to measure serum cytokines, serum APPs, and immune cell populations. These larger numbers were used to account for the greater variability between mice in these experiments. We follow standards in the field when choosing sample sizes for in vitro and in vivo experiments (Yadav et al Nature 2014, Kreiter et al Nature 2016, Gitlin et al Nature 2020, Kayagaki et al Nature 2021).
Data exclusions	No data were excluded from analyses.
Replication	Whenever possible, readouts were performed with at least 3 animals of a given genotype and all attempts at replication were successful. As indicated in figure legends, independent experiments and biological replicates were used to ensure reproducibility of results. In vitro human data is represented as the mean or median value of 2 or 3 technical replicates for a given donor. Each experiment was replicated 2-4 times with biologically independent samples.
Randomization	Samples or mice were grouped according to genotype or treatment, and thus not randomized. Where possible, animals were age- and sex matched. When inhibitors or blocking antibodies were used in human PBMC experiments, samples from the same donor were directly compared.
Blinding	Mice were selected and treated by the same individual, so blinding to allocation and data collection/analysis was not possible.

Reporting for specific materials, systems and methods

We require information from authors about some types of materials, experimental systems and methods used in many studies. Here, indicate whether each material, system or method listed is relevant to your study. If you are not sure if a list item applies to your research, read the appropriate section before selecting a response.

Materials & experimental systems

n/a	Involved in the study
☐	☒ Antibodies
☐	☒ Eukaryotic cell lines
☒	☐ Palaeontology and archaeology
☐	☒ Animals and other organisms
☐	☒ Human research participants
☐	☒ Clinical data
☒	☐ Dual use research of concern

Methods

n/a	Involved in the study
☒	☐ ChIP-seq
☐	☒ Flow cytometry
☒	☐ MRI-based neuroimaging

Antibodies

Antibodies used

Fluorochrome and target (clone/manufacturer/catalogue number/lot number/dilution/extra- or intracellular):

Purified Rat Anti-Mouse CD16/CD32 (2.4G2/BD/553141/7248907/1:200/extracellular)
FITC anti-CD169 (3D6.112/Biolegend/142406/B185155/1:100/extracellular)
PE anti-IL-1a (ALF-161/ eBioscience/12-7011-82/2021232/1:50/intracellular)
PerCP-Cy5.5 anti-CD3 (17A2/ Biolegend/100218/B233420/1:100/extracellular)
BUV395 anti-B220 (RA3-6B2/BD/563793/8120543/1:200/extracellular)
PE anti-NK1.1 (PK136/Biolegend/108707/B248845/1:100)
BV510 anti-CD11c (N418/ Biolegend/117338/B290360/1:100/extracellular)
BUV737 anti-CD4 (GK1.5/BD/ 612761/9290412/1:100/extracellular)
VioBlue anti-CD11b (M1/70.15.11.5/Miltenyi Biotec/130-113-238/5191212813/1:100/extracellular)
APC anti-CD115 (AFS98/Biolegend/ 135510/B241282/1:100/extracellular)
AF488 anti-CD11b (M1/70/Biolegend/ 101219/B248739/1:200/extracellular)
PeCy7 anti-pro-IL-1b (NJTEN3/eBioscience/ 25-7114-82/2016884/1:100/intracellular)
BV711 anti-F4/80 (BM8/Biolegend/123147/B301622/1:100/extracellular)
AF647 anti-Siglec-F (E50-2440/BD/ 562680/9185572/1:100/extracellular)

AF700 anti-Ly-6C (HK1.4/Biolegend/128024/B297755/1:100/extracellular)
PeCy7 anti-CD8a (53-6.7/BD/552877/9186813/1:200/extracellular)
BV785 anti-Ly-6G (1A8/Biolegend/127645/B295080/1:100/extracellular)
APC anti-CD209b (22D1/eBioscience/17-2093-82/4326927/1:100/extracellular)
FITC PD-1 (29F.1A12/Biolegend/135214/B277058/1:100/extracellular)
AF700 CD8 (KT15/BioRad/MCA609A700/151453/1:100/extracellular)
V500 CD90.1 (53-2.1/Biolegend/561616/9289835/1:100/extracellular)
APC-Cy CD4 (GK1.5/BD Biosciences/552051/9165919/1:100/extracellular)
APC-H7 CD19 (1D3/BD Biosciences/560143/9016562/1:200/extracellular)
BUV395 KLRG1 (2F1/BD Biosciences/740279/0155219/1:100/extracellular)
PerCP-eFluor710 CD127 (SB/199/Invitrogen/46-1273-82/2222040/1:100/extracellular)
PE TCF1/TCF7 (C63D9/Cell Signaling Technology/14456S/12/1:50/intracellular)
AF488 IFNg (XMG1.2/Biolegend/505813/B282839/1:200/intracellular)
BUV395 TCRb (H57-597/BD Biosciences/742485/9249141/1:200/extracellular)
PeCy7 CD8 (53-6.7/BD Biosciences/552877/9039618/1:200/extracellular)
BV510 B220 (RA3-6B2/Biolegend/103248/B291212/1:200/extracellular)
BV421 TNF-a (MP6-XT22/ Biolegend/506328/B274627/1:200/intracellular)
BV785 CD4 (RM4-5/Biolegend/100552/B301975/1:200/extracellular)
APC CD107a (1D4B/Biolegend/121614/B247105/1:400/intracellular)
PE IL-1R1 (JAMA-147/Biolegend/113505/B314158/1:100/extracellular)
BV421 IL-1R2 (4E2/BD Biosciences/562926/1027815/1:100/extracellular)
Purified Anti-CD3/anti-LyPD1 TDB (2C11/Genentech/NA/pur#47392/NA/extracellular)
InVivoMAb rat IgG2a isotype control (2A3/BioXCell/BE0089/796721M2/NA/extracellular)
InVivoPlus anti-mouse anti-Ly6G (1A8/BioXCell/BP0075-1/737720J1/NA/extracellular)
Purified anti-hIL-1β-IgG (4H5/InvivoGen/mabg-hil1b-3/4H5-39-01)
Purified mouse Control IgG1 (T8E5/InvivoGen/mabg1-ctrlm/CT1-39-02)
Human TruStain FcX™ (NA/Biolegend/422302/B290761/1:20/extracellular)
PerCP-Vio700 anti-CD14 (TÜK4/Miltenyi Biotec/130-097-539/5171009330/1:5/extracellular)
PE anti-CD66b (G10F5/Biolegend//305106/B258031/1:20/extracellular)
APC-H7 anti-CD19 (SJ25C1/BD/560177/7341759/1:20/extracellular)
V500 anti-HLA-DR (G46-6/BD/ 561224/8260613/1:20/extracellular)
APC anti-CD14 (M5E2/Biolegend/301808/B259538/1:20/extracellular)

Validation

Primary antibodies used for flow cytometry and blocking assays are commercially available and validated by vendors for human proteins (used in our in vitro assays and flow cytometry) or murine proteins (used in our in vivo experiments and in flow cytometry).

APC anti-CD14 (M5E2/Biolegend/301808/B259538/1:20/extracellular) has been validated by Biolegend to recognize human, cynomolgus and rhesus macaque CD14: https://www.biolegend.com/en-us/products/apc-anti-human-cd14-antibody-793?Clone=M5E2

Purified Anti-CD3/anti-LyPD1 TDB (2C11/Genentech/NA/pur#47392/NA/extracellular) has been characterized and validated by Lo et al Mol Cancer Ther 2021 https://mct.aacrjournals.org/content/20/4/716.long

Eukaryotic cell lines

Policy information about cell lines

Cell line source(s)	ID8/LyPD1 cells have been generated at Genentech (Lo, A. A. et al, 2021. Mol Cancer Ther 20: 1–10).
Authentication	Cell line was verified using short tandem repeat (STR) profiling (Promega PowerPlex 16 System).
Mycoplasma contamination	Cells were negative for mycoplasma.
Commonly misidentified lines (See ICLAC register)	Not used.

Animals and other organisms

Policy information about studies involving animals; ARRIVE guidelines recommended for reporting animal research

Laboratory animals	C57BL/6J mice (stock 000664) and Il1rn-/- mice (B6.129S-Il1rntm1Dih/J, stock 004754) were purchased from the Jackson Laboratory. Il1r1-/- mice were obtained from Jackson Laboratories (B6.129S7-Il1r1tm1Imx/J, stock 003245) and back-crossed for 8 generations to C57BL/6J mice (Jackson Laboratories). Nlrp3-/- mice (also known as Cias1-/- mice) have been described (Mariathasan et al, 2006. Nature 440: 228–232). Gsdmd-/- mice have been described (Kayagaki, N. et al, 2015. Nature 526, 666–671). Age-matched (5–15 weeks) female animals were used throughout all experiments. Mice were maintained in a specific pathogen-free facility, in individually ventilated cages within animal rooms maintained on a 14:10-hour, light:dark cycle. Animal rooms were temperature and humidity-controlled, between 68-79°F and 30-70% respectively, with 10 to 15 room air exchanges per hour.
Wild animals	The study did not involve wild animals.
Field-collected samples	The study did not involve samples collected from the field.
Ethics oversight	All animal studies were reviewed and approved by Genentech's Institutional Animal Care and Use Committee (IACUC).

Note that full information on the approval of the study protocol must also be provided in the manuscript.

Human research participants

Policy information about studies involving human research participants

Population characteristics	Peripheral blood was used from healthy human donors participating in Genentech blood donor program. Buffy coats from anonymous donors were used. As such, covariate-relevant participant characteristics such as age and gender are not available.
Recruitment	Participation in Genentech blood donor program is voluntary and on a as basis. Donors receive a compensation based on the type and volume of sample donated. Although self-selection bias may be present and is difficult to exclude, it is unlikely to affect our conclusions because we compared PBMCs treated with RNA-LPX and inhibitors or blocking antibodies to RNA-LPX only treated cells from the same donor (each experiment was performed with at least 2 independent donors and each experiment was replicated 2-4 times). No significant biases have been identified, and we have consistently observed the expected donor-to-donor variability in our assays (which only affects the total but not the relative magnitudes of cytokine release between different donor cells following stimuli).
Ethics oversight	Written, informed consent was obtained from participants. This protocol was approved by the Western Institutional Review board.

Note that full information on the approval of the study protocol must also be provided in the manuscript.

Clinical data

Policy information about clinical studies

All manuscripts should comply with the ICMJE guidelines for publication of clinical research and a completed CONSORT checklist must be included with all submissions.

Clinical trial registration	ClinicalTrials.gov Identifier: NCT03289962.
Study protocol	The full clinical study protocol is not published online, but a comprehensive description of the clinical trial design, eligibility criteria and endpoints is available at https://www.clinicaltrials.gov/ct2/show/NCT03289962.
Data collection	We analyzed pre- and post-treatment plasma levels of IL-1b, IL-1a and IL-1ra in a cohort of 9 patients with advanced malignancies receiving individualized tumor neoantigen-encoding RNA-LPX (RO7198457 or Autogene Cevumeran) in a phase 1b dose-escalation trial (NCT03289962). RO7198457 was administered intravenously at a dose of 25 ug and atezolizumab at a dose of 1200 mg. Blood samples were obtained before vaccination (pre-dose), and at 4-6 hours and 24 hours after RO7198457 administration. Plasma cytokines were measured from 9 patients shown in Figures 1i and 3d (sample selection was based on plasma availability and existing ELISPOT data, while excluding patients that had received steroids at the time of vaccination). Plasma was prepared at clinical sites and shipped on dry ice to the central laboratory on the day of blood draw. When sites were not able to ship samples on the day of draw, plasma samples were kept in a deep freezer (-80C) and shipped next business day to the Central Lab . Central Lab batch shipped samples monthly to Myriad-RBM (Austin, TX, USA), where testing and data collection was performed. Plasma samples were stored in -80C, thawed on the day of testing, and run using IL-1b Simoa assay (Quanterix, dilution factor 2) and DiscoveryMAP Multiplexes (Myriad RBM, dilution factor 5).
Outcomes	Primary and secondary outcomes of this phase 1b trial are available at https://www.clinicaltrials.gov/ct2/show/NCT03289962. Primary Outcome Measures: Percentage of Participants with Dose-Limiting Toxicities (DLTs) [Time Frame: Phase 1a: Days 1 to 14 / Phase 1b: Days 1 to 21] MTD/Recommended Phase 2 Dose (RP2D) of Autogene Cevumeran [Time Frame: Phase 1a: Days 1 to 14 / Phase 1b: Days 1 to 21] Percentage of Participants with Adverse Events (AEs) [Time Frame: Baseline up to end of the study (up to approximately 3 years)] Percentage of Participants with Immune-Mediated Adverse Events (imAEs) [Time Frame: Baseline up to end of the study (up to approximately 3 years)] Percentage of Participants by Number of Treatment Cycles Received [Time Frame: Baseline up to end of the study (up to approximately 3 years)] Dose Intensity of Autogene Cevumeran [Time Frame: Baseline up to end of the study (up to approximately 3 years)] Change from Baseline in Targeted Vital Signs [Time Frame: Baseline up to end of study (up to approximately 3 years)] Change from Baseline in Targeted Clinical Laboratory Test Results [Time Frame: Baseline up to end of study (up to approximately 3 years)] Change from Baseline in ECGs [Time Frame: Baseline up to end of study (up to approximately 3 years)] Secondary Outcome Measures: Percentage of Participants with Objective Response of Complete Response (CR) or Partial Response (PR) According to Response Evaluation Criteria for Solid Tumors Version 1.1 (RECIST v1.1) [Time Frame: Baseline until 90 days after last dose or initiation of another systemic anti-cancer therapy, whichever occurs first (up to approximately 3 years)] Duration of Response (DoR) According to RECIST v1.1 [Time Frame: From first occurrence of a documented objective response (CR or PR) until disease progression or death due to any cause, whichever occurs first (up to approximately 3 years)] Percentage of Participants with Objective Response of CR or PR According to Immune-Modified RECIST [Time Frame: Baseline until 90 days after last dose or initiation of another systemic anti-cancer therapy, whichever occurs first (up to approximately 3 years)] DoR According to Immune-Modified RECIST [Time Frame: From first occurrence of a documented objective response (CR or PR) until disease progression or death due to any cause, whichever occurs first (up to approximately 3 years)] Progression-Free Survival (PFS) According to RECIST v1.1 [Time Frame: Baseline until 90 days after last dose or initiation of another

systemic anti-cancer therapy, whichever occurs first (up to approximately 3 years)]
Overall Survival (OS) [Time Frame: Baseline until 90 days after last dose or initiation of another systemic anti-cancer therapy, whichever occurs first (up to approximately 3 years)]
Percentage of Participants with Anti-Drug Antibodies (ADAs) to Atezolizumab [Time Frame: Pre-infusion (0 hr) until 2 months post treatment discontinuation (up to approximately 3 years)]

The results of this phase 1b study have been presented in the AACR Annual Meeting 2020, abstract is available at https://cancerres.aacrjournals.org/content/80/16_Supplement/CT301

The desired outcome of measuring cytokine levels in 9 patient samples from this phase 1b trial (sample selection criteria described above) was to study whether we can detect IL-1 family members in vivo following clinical RNA-LPX treatment.

Flow Cytometry

Plots

Confirm that:

☒ The axis labels state the marker and fluorochrome used (e.g. CD4-FITC).

☒ The axis scales are clearly visible. Include numbers along axes only for bottom left plot of group (a 'group' is an analysis of identical markers).

☒ All plots are contour plots with outliers or pseudocolor plots.

☒ A numerical value for number of cells or percentage (with statistics) is provided.

Methodology

Sample preparation	Spleens were harvested in cold PBS and single-cell suspensions were generated by mashing the spleen tissue through a 70 um cell strainer (BD Falcon) in Hank's based Cell Dissociation Buffer (Gibco) supplemented with Liberase (Roche) and DNase I (ThermoFisher). Red blood cells were lysed with ACK lysis buffer (Gibco). Single-cell suspensions were incubated in FACS buffer (PBS supplemented with 0.5 % BSA and 0.05% Sodium Azide) containing anti-mouse CD16/CD32 (Mouse Fc Block, BD) or Human TruStain FcX (Human Fc Block, Biolegend) for 10 min prior to and during staining with the indicated antibodies. Intracellular Fixation & Permeabilization Buffer Set (88-8824-00, eBioscience) was used for intracellular staining of IL-1a and IL-1b. Foxp3 / Transcription Factor Staining Buffer Set (00-5523-00, eBioscience) was used for intranuclear staining of TCF-1. Cells were stained on ice for extracellular markers for 20-30 min followed by staining for intracellular markers for 60 min, and filtered using 30-40 um filter plates (PALL).
Instrument	BD FACSymphony (BD Biosciences)
Software	Data was acquired using BD FACSDiva software v8.0, and analyzed using FlowJo 10.7.1.
Cell population abundance	No sorting was performed.
Gating strategy	Leukocytes were identified based on their forward scatter (FSC-A) and side scatter (SSC-A) profiles. Dead cells and cell aggregates were excluded from analyses by Fixable Viability Dye eFluor 780 (eBioscience) or LIVE/DEAD™ Fixable Blue (Dead Cell Stain Kit for UV excitation, Invitrogen) staining and FSC-A/FSC-H characteristics. Gating strategies to identify different myeloid and lymphocyte cell subsets among live blood leukocytes are shown in Extended Data Fig. 6a. Gating strategy to identify different myeloid cell subsets among live splenocytes is shown in Extended Data Fig. 8a. Gating strategy to identify neoantigen-specific T cells is shown in Figure 4d. Gating strategy to identify IL-1b+ or IL-1a+ cells within myeloid cell subsets among live splenocytes is shown in Extended Data Fig. 2c, e and 8b.

☒ Tick this box to confirm that a figure exemplifying the gating strategy is provided in the Supplementary Information.